Quantifying bamboo coral growth rate nonlinearity with the radiocarbon bomb spike: A new model for paleoceanographic chronology development

Frenkel, M. M.[1], LaVigne, M.[1], Miller, H. R.,[1] Hill, T.M.,[2,3] McNichol, A.[4], Lardie Gaylord, M.[4]

[1] Earth and Oceanographic Science Department, Bowdoin College, Brunswick, Maine, USA

[2] Bodega Marine Laboratory, University of California, Davis, Bodega Bay, CA

[3] Department of Earth and Planetary Sciences, University of California Davis, Davis, CA

[4]National Ocean Sciences Accelerator Mass Spectrometry Facility, Woods Hole Oceanographic Institution, Woods Hole, MA

Corresponding author: Megan Maria Frenkel, Department of Earth and Environmental Sciences, Lamont-Doherty Earth Observatory of Columbia University, 61 Route 9W, P.O. Box 1000, Palisades, NY, 10964, USA. mmf2171@columbia.edu

Keywords: bamboo coral; gorgonin; paleoceanography; chronologies; radiocarbon; growth rate; 14C nuclear bomb spike

1. ABSTRACT

Bamboo corals, long-lived cold water gorgonin octocorals, offer unique paleoceanographic archives of the intermediate ocean. These *Isididae* corals are characterized by alternating gorgonin nodes and high Mg-calcite internodes, which synchronously extend radially. Bamboo coral calcite internodes have been utilized to obtain geochemical proxy data, however, growth rate uncertainty has made it difficult to construct precise chronologies for these corals. Previous studies have relied upon a tie point from records of the anthropogenic $\Delta^{14}C$ bomb spike preserved in the gorgonin nodes of live-collected corals to calculate a mean radial extension rate for the outer ~50 years of skeletal growth. Bamboo coral chronologies are typically constructed by applying this mean extension rate to the entire coral record, assuming constant radial extension with coral age. In this study, we aim to test this underlying assumption by analyzing the organic nodes of six California margin bamboo corals at high enough resolution (<0.5 mm) to identify the $\Delta^{14}C$ bomb spike, including two tie points at 1957 and 1970, plus coral collection date (2007.5) for four samples. Radial extension rates between tie points ranged from 10 to 204 μm/year, with a decrease in growth rate evident between the 1957-1970 and 1970-2007.5 periods for all four corals. A negative correlation between growth rate and coral radius ($r = -0.7$; $p = 0.03$) was determined for multiple bamboo coral taxa and individuals from the California margin, demonstrating a decline in radial extension rate with specimen age and size. To provide a mechanistic basis for these observations, a simple mathematical model was developed based on the assumption of a constant increase in circular cross sectional area with time to quantify this decline in radial extension rate with coral size between chronological tie points. Applying the area-based model to our $\Delta^{14}C$ bomb spike time series from individual corals improves chronology accuracy for all live-collected corals with complete $\Delta^{14}C$ bomb spikes. Hence, this study provides paleoceanographers utilizing bamboo corals with a method for reducing age model uncertainty within the anthropogenic bomb spike era (~1957-present). Chronological uncertainty is larger for the earliest portion of coral growth, particularly for skeleton precipitated prior to bomb spike tie points, meaning age estimations for samples living before 1957 remain uncertain. Combining this technique with additional chronological markers could improve age models for an entire bamboo coral. Finally, the relative consistency in growth rate in similarly-aged corals of the same depth and location supports the hypothesis that skeletal growth may be limited by local environmental conditions.

2. INTRODUCTION:

Sparse and incomplete instrumental oceanographic measurements are unable to provide the continuous high-resolution datasets required to study the scale and nature of pre-industrial climate variability. The current paradox related to these instrumental records is that some of the most undersampled regions of the ocean are quickly becoming the most important regions to study. For example, due to climate change, a "lethal trio" of acidification, warming and deoxygenation is projected to have a dramatic effect on ocean ecosystems at intermediate depths (~800-2200 m; Hill et al., 2014) along zones of upwelling where hypoxic conditions are already established (Keeling et al., 2010; Stramma et al., 2010; Bijma et al., 2013). However, predicting the extent and severity of this 'lethal trio' into the future requires greater understanding of how these upwelling zones have changed in the past. Such questions have spurred an interest in high-resolution (i.e., annual-decadal resolution) biogeochemical proxy records as a means to circumvent reliance on instrumental data. These records require two components: (1) high-resolution proxy archives and, the focus of this paper, (2) accurate and high-precision chronologies.

One archive of intermediate water conditions that is gaining increasing attention from the paleoceanography community is bamboo coral. Bamboo corals (for example, genera *Isidella, Keratoisis,* and *Lepidisis)* are a group of gorgonin octocorals named for their alternating high-magnesium calcite (7-10 mol% $MgCO_3$) internodes and proteinaceous gorgonin nodes that resemble a bamboo stalk (Grant, 1976). Because the calcitic skeleton and organic nodes simultaneously extend radially, these corals provide the opportunity to study temporally linked organic and inorganic material (Roark et al., 2005; Watling et al., 2011; Hill et al., 2014). Previous work has also demonstrated that bamboo corals precipitate their inorganic skeleton from ambient dissolved inorganic carbon (DIC; Roark et al., 2005; Hill et al., 2011; Farmer et al., 2015a), while their nodes are composed of carbon derived from particulate organic matter (POM) recently exported from the surface (Griffin and Druffel, 1989; Roark et al., 2005; Hill et al., 2014; Schiff et al., 2014), meaning that a single bamboo coral sample offers a record of temporally coincident surface and deep-water conditions.

A bamboo coral's alternating calcitic-gorgonin skeleton is nonliving, providing only the supporting structure for the living community of polyps embedded into a common coenenchymal tissue (Fabricius, 2011; Watling et al., 2011). Colonizing intermediate water depths (most often 400 to 3000 m), these deep-sea organisms are well-adapted passive suspension feeders that live on hard substrates (i.e., ridges, elevated rock ledges, bedrock walls and boulders) and biodiversity is particularly high on seamounts where sedimentation is

low or where currents prevent the accumulation of fine-grained sediment (e.g., Edinger et al., 2011; Lacharité and Metaxas, 2013). Although access to adequate food supply is also critical, these organisms can be found in most ocean basins and can live up to 200-400 years (Thresher et al., 2004; Andrews et al., 2005; Watling et al., 2011).

The combination of longevity, geographic abundance, thermal tolerance and broad depth preferences poses bamboo corals as promising decadal-centennial scale archives of intermediate water conditions over the past century or more (e.g., Thresher et al., 2004; Sherwood et al., 2009; LaVigne et al., 2011; Hill et al., 2012). Existing literature has already begun to evaluate the reliability and fidelity of proxy data from bamboo coral samples. Early studies of the trace-elemental composition of bamboo coral calcite illustrated the potential for Ba, Mg, and Sr to be reliably recorded in coral carbonate (Thresher et al., 2009; Sinclair et al., 2011, Hill et al., 2012; Prouty et al., 2015). This work was followed by calibration studies of calcite Ba/Ca, a potential proxy for oceanic upwelling and refractory nutrient dynamics (LaVigne et al., 2011; Thresher et al., 2016), stable isotopic temperature tracers using the $\delta^{18}O$, $\delta^{13}C$ "lines method" (Hill et al., 2011, Kimball et al., 2014, Saenger et al., 2016), and studies investigating the potential for bamboo coral calcite B/Ca and $\delta^{11}B$ to record ambient deep-sea pH (Farmer et al., 2015a). Carbon and nitrogen isotopes preserved in bamboo coral gorgonin nodes have also been used to reconstruct past changes in surface production and organic carbon remineralization (Hill et al., 2014; Schiff et al., 2014).

Though bamboo corals represent a promising climate archive, generating precise chronologies for these samples has proven challenging (Prouty et al., 2015). Although corals grow both vertically and radially, radial extension rates are the focus of chronological efforts because elemental data is most often obtained from a horizontal cross section of the coral (Roark et al., 2005). However, unlike scleractinian surface corals, bamboo corals do not offer a visual means of determining age and growth rate. While light-dark banding patterns in calcitic thin sections are often visible using light microscopy, inconsistent and irregular banding, and difficulty in distinguishing individual bands renders this technique unreliable (Andrews et al., 2005; Roark et al., 2005; Noé and Dullo, 2006; LaVigne et al., 2011), particularly because there is currently no consensus that these bands represent annual growth increments in all bamboo corals (Roark et al., 2005; Tracey et al., 2007; Prouty et al., 2015). Additionally, unlike aragonitic surface (e.g., Cobb et al., 2003) and deep-sea corals (e.g. Cheng et al., 2000), bamboo coral calcite does not contain enough uranium for precise U/Th dating (~0.03 ppm, Sinclair et al., 2011; Thresher et al., 2004). Although radioactive decay of ^{210}Pb naturally incorporated into the coral

calcite from seawater has been successfully utilized to determine age and growth of deep-sea corals (Druffel et al., 1990; Andrews et al., 2002), including bamboo corals (Andrews et al., 2005; Andrews et al., 2009; Sinclair et al., 2011), this method requires a relatively large sample size, would not be suited for longer-lived bamboo coral samples (older than ~100 years), and may be influenced by changes in environmental ^{210}Pb (Andrews et al., 2009). Meanwhile, more recent efforts aimed at using calcite $\Delta^{14}C$ referenced to the $\Delta^{14}C$ of dissolved inorganic carbon in ambient seawater were challenged by evidence of complicating factors including water mass variability and coral ontogeny (Farmer et al., 2015b). Given the difficulties associated with these more traditional methods, previous work has investigated amino acid racemization and quasi-regular peaks in Sr/Ca as a means of calculating coral age, though these dating methods also prove challenging (Sherwood et al., 2006; Thresher et al., 2009).

One promising method for constructing bamboo coral chronologies takes advantage of the rise of atmospheric radiocarbon ($\Delta^{14}C$ values ≥-85‰) after nuclear weapons testing in the 1950s and early 1960s and the ocean surface DIC signature recorded in coral nodes (Roark et al., 2005; Sherwood et al., 2009; Hill et al., 2014; Prouty et al., 2015). Previous work has shown that core to rim $\Delta^{14}C$ profiles of bamboo coral nodes reflect a radiocarbon plateau in the pre- bomb record, followed by a marked increase in $\Delta^{14}C$ reflecting the initiation of weapons testing (Roark et al., 2005; Hill et al., 2014). Based on proximal rockfish otolith records from the Gulf of Alaska, the first expression of this $\Delta^{14}C$ rise in northeast Pacific surface waters can be assigned a date of 1957 ± 2 years and the $\Delta^{14}C$ maximum is most often assigned a date of 1970 for samples derived from the northeast Pacific (e.g. Kerr et al., 2004; Kerr et al., 2005; Roark et al., 2005; Hill et al. 2014; Schiff et al., 2014). The year of live coral collection provides a third tie point. Using the radial distances between tie points, growth rates can be calculated for each growth interval and applied as a chronology assuming a constant radial growth rate with coral age.

It is important to note that these radiocarbon-based chronology constructions rely on two key assumptions. The first assumption is that POM and zooplankton carrying the $\Delta^{14}C$ signal from the surface are exported to the deep sea with minimal delay (Hill et al., 2014). This notion is supported by the fact that sinking particle rates in the North Pacific can reach 175 to 300 m/day during periods of peak primary production, indicating that corals at 1,000 m depths may feed on particles less than 1 week old (Wong et al., 1999; Hill et al., 2014). The second commonly utilized assumption is that corals exhibit a constant radial extension rate over their lifespan and that the radial extension rate between the 1957 tie point in the bomb spike record and the

collection date can be applied to the entirety of a coral record (Roark et al., 2005; Andrews et al., 2009; Sherwood and Edinger, 2009; Hill et al., 2014; Schiff et al., 2014). Despite the uncertainties inherent in this methodology, bomb $\Delta^{14}C$ has provided the most accurate chronologies for bamboo coral records to date.

Nevertheless, preliminary evidence for growth rate nonlinearity has recently been identified in bamboo corals, calling the second assumption into question (Farmer et al., 2015b). An early study of *Muricea californica* and *Muricea frutiocosa*, two entirely gorgonin coral taxa living at shallow depths where seasonality results in annual rings, interpreted variable growth banding as evidence of inconsistent growth rates (Grigg, 1974). The skeletal calcite growth mode put forward by Noé and Dullo (2006), which suggests a fundamental transition in a coral's crystalline fabric from radial fibrous to tangential granular crystals as it progresses from the juvenile to the adult growth phase, also proposes a change from faster to slower radial extension rates with coral age. Additionally, previous work has implicated nonlinear radial growth as an explanation for deviations in the $\Delta^{14}C$ profile of the deep water coral *Paragorgia aborea* from reference $\Delta^{14}C$ profiles (Sherwood and Edinger, 2009). Most recently, radial extension rate determinations based on calcite $\Delta^{14}C$ have illustrated the potential for extension rate to decrease by as much as a factor of three over a 6mm range (Farmer et al., 2015b). Finally, Thresher et al. (2016) found evidence for linear and non-linear fits between calcite radiocarbon dates and distance from the calcite core of Tasmanian bamboo corals. Taken together, these studies provide preliminary evidence for declines in radial extension rate with coral age that challenges the notion of radial growth rate constancy over time.

Because growth rate nonlinearity could lead to under-or over-estimations of coral age, the emerging evidence of bamboo coral growth rate non-linearity suggests that the assumption of constant growth rate with coral age should be tested and refined. Additionally, the fact that previous studies have relied upon constant-growth-rate chronologies due to low sampling resolution leaves room for future work to improve bamboo coral chronology construction using $\Delta^{14}C$ records that can resolve multiple tie points.

Higher resolution $\Delta^{14}C$ bomb-spike analyses may be achieved with recently developed techniques. Methods for preparing coral gorgonin samples for $\Delta^{14}C$ analysis have evolved from milling a transect of the gorgonin disk (Roark et al., 2005), to a preparation technique that involves peeling individual concentric gorgonin layers (Sherwood and Edinger, 2009; Burke et al., 2010; Schiff et al., 2014, Hill et al., 2014). These gorgonin "peels" can be analyzed using 'reconnaissance' radiocarbon analysis, a recently developed method for conducting age surveys of deep-sea aragonitic corals (Xu et al., 2007; Burke et al., 2010). Traditional graphite

160 production methods, such as hydrogen reduction of CO_2 with iron or cobalt catalyst, are precise, accurate, and
161 widely applicable, but can be time consuming and expensive. However, the new 'reconnaissance' procedure
162 utilizes an elemental analyzer to rapidly convert samples to CO_2, and has been shown to minimize the expense
163 of $\Delta^{14}C$ measurements, while producing high quality graphite for precise (2-3‰) and accurate radiocarbon
164 measurements (Xu et al. 2007; Burke et al., 2010). Frequent sampling along a gorgonin node, in conjunction
165 with this 'reconnaissance' analysis method, is ideal for the task of reconstructing a complete $\Delta^{14}C$ profile for
166 bamboo coral samples.

167 Given the current gaps in literature regarding bamboo coral chronologies, this study sought to use the
168 'reconnaissance' radiocarbon technique at high sampling resolution to construct the anthropogenic $\Delta^{14}C$ bomb
169 spike in six bamboo coral samples. By determining two radial extension rates for multiple specimens, the
170 convention of applying a single growth rate to an entire coral lifespan was tested. Given evidence that
171 challenged this assumption, a reasonable simple mathematical model for coral growth over time is proposed.
172

173 **3. METHODS**

174 *3.1 Samples*

175 The six coral samples used in this study were collected from Pioneer and Davidson Seamounts (839-1500 m
176 depth) on the California margin (Table 1, Fig. 1). The samples were collected in June, 2007 using the ROV
177 Tiburon on the Monterey Bay Aquarium Research Institute (MBARI) vessel R/V Western Flyer (Hill et al.,
178 2012, Hill et al., 2014). Upon collection, samples were classified as *Isidella* and *Keratosis* genera, though
179 uncertainties regarding more specific taxonomic determinations preclude definite identifications (Hill et al.,
180 2014, France, 2007). All corals sampled were of branching morphologies. Upon collection, corals were
181 identified as "live" or "dead", based on the presence or absence of polyp material on the skeleton (Hill et al.,
182 2014). Polyps were removed from the live specimens upon collection and the skeleton was archived dry at UC
183 Davis Bodega Marine Laboratory.

184

185 *3.2 Sample Preparation for Radiocarbon Analysis*

186 Prior to analysis, all sampling supplies (i.e. forceps and glassware) were cleaned with the following
187 protocol: (1) "Sparkleen" lab soap (Fisher Scientific) wash, (2) deionized water rise (3x), (3) 10% HCl rinse (1x),

and (4) ultrapure (18.2 MΩ-cm) water rinse (3x). Cleaned supplies and aluminum foil were then baked in a muffle furnace at 550°C for one hour to remove any residual carbon.

Gorgonin nodes were detached from adjoining calcitic internodes using a Dremel circular cutting tool. Samples were then placed in 10% HCl until most of the remaining calcite had dissolved (up to a 4 hours). For recalcitrant remaining calcite, samples were sonicated for up to two hours. The isolated node was rinsed with deionized water and sampled radially at ~0.5 mm resolution by peeling layers of gorgonin using a razor blade and forceps under a stereomicroscope. The node was measured with a digital micrometer under the stereo-microscope along the longest and shortest radii before and after each peeling. In later analysis, the sampling distance measured along all radii were averaged to identify each peel's thickness and radial distance. The resulting gorgonin 'peels' were dried at approximately 90°C in a drying oven for 24 hours.

In order to obtain the most representative sample, subsamples were collected from large peels (>~2-3 mg). These subsamples (<0.5 mg pieces) were cut from each side of the peel and recombined (2-3 mg total) for analysis.

3.3 Radiocarbon data collection

Radiocarbon analyses were conducted at the National Oceanic Science Accelerator Mass Spectrometry (NOSAMS) Facility at the Woods Hole Oceanographic Institution (WHOI). The procedure was adapted from the "reconnaissance" method developed for aragonite by Burke et al. (2011), with the following steps: (1) combustion of each individual gorgonin peel (~1 mg carbon) by an elemental analyzer (Elementar vario EL cube), (2) removal of the helium carrier gas and conversion of gaseous carbon dioxide to solid CO_2 in liquid nitrogen in a reagent tube containing 30-35 mg zinc (reducing agent), 15-20 mg titanium hydride (H_2 source, reducing agent) and 3.5 mg iron (catalyst), and (3) reduction of the resulting carbon dioxide to graphite via high temperature in a furnace at 500° C for 3 hours and 550°C for 4 hours (Xu et al., 2007). While this technique provides absolute ages with lower precision and is not suitable for small or particularly old samples, it requires only a fraction of the time and cost of standard organic carbon methods, can be easily set up, and hence can be used to rapidly analyze many samples (Xu et al., 2007; Burke et al., 2010).

The resulting graphite samples were stored in the sealed combusted reaction tubes until they were pressed into targets and analyzed with the NOSAMS Tandetron Accelerator-Mass Spectrometer (AMS) (von

Reden et al., 2004; Longworth et al., 2015). To calibrate the instrument and ensure quality control, a primary standard (OX II oxalic acid), three secondary standards (C-3 cellulose, C7 oxalic acid, FIRI H wood), and one blank (Acetanilide) were analyzed alongside the coral samples.

Data were originally provided as a blank-corrected fraction modern (F_m), a measurement of the deviation of the $^{14}C/^{12}C$ ratio of the sample from "modern," defined as 95% of the radiocarbon concentration (in AD 1950) of NBS Oxalic Acid I (SRM 4490B, OX1) normalized to $\delta^{13}C_{VPDB}$=-19 per mil (Olsson, 1970). Internal statistical error (E) was calculated using the total number (n) of ^{14}C counts measured for each target ($E = 1/\sqrt{n}$) and external error was calculated from the reproducibility of 10 separate sample $^{14}C/^{12}C$ measurements obtained over the course of a run. The final error associated with fraction modern values was determined from the larger of the internal or external errors. $\Delta^{14}C$ values were then calculated using equation (1) as defined in Stuiver and Pollach (1977), where λ is 1/(true mean-life) of radiocarbon (1/8267 = 0.00012097), and Y_c is year of collection. (http://www.whoi.edu/nosams/radiocarbon-data-calculations for more information or von Reden et al., 2004; Longworth et al., 2015). In this study, final error on $\Delta^{14}C$ values ranged from approximately 0.01-0.3‰, or roughly 0.20-0.40% of the $\Delta^{14}C$ measurement (see Supplemental Table S1 for unprocessed $\Delta^{14}C$ dataset).

$$\Delta^{14}C = [Fm * e^{\lambda(1950 - Yc)} - 1] * 1000 \quad (1)$$

3.4 Radiocarbon Data Processing

Features of the bomb spike in the gorgonin radiocarbon record for coral T1102 A12, the specimen exhibiting the highest resolution $\Delta^{14}C$ bomb-spike, were first identified as follows: the first data point to rise above pre-bomb values ($\Delta^{14}C$ = -83.12‰) was assigned a date of 1957 and the first point to reach the maximum $\Delta^{14}C$ value in each curve was assigned a date of 1970 (Fig. 2b). A third tie point was assigned to the outer edge of the coral based on the date of live coral collection (2007.5; Fig. 2). The dates for the first two tie points were selected by identifying the same features in independently dated Gulf of Alaska yelloweye rockfish (Kerr et al., 2004) and Pacific halibut (Piner and Wischniowski, 2004) otolith reference records, which represent $\Delta^{14}C$ of surface water DIC from which coral gorgonin signal is ultimately derived (Fig. 3b; Roark et al., 2005; Hill et al., 2014). The $\Delta^{14}C$ values, as well as the timing of the $\Delta^{14}C$ rise, agree very well between the rockfish and halibut records (Fig. 3b). The maximum $\Delta^{14}C$ value is first reached in 1970 in both records; after this date, however, the reference records begin to diverge as $\Delta^{14}C$ declines to current levels. We note that the differences

between these records after the 1970 tie point do not impact our growth rate calculations as our coral data are not chronologically tied to this feature of the bomb-spike. Additional recently published otolith $\Delta^{14}C$ profiles from the northeast Pacific exhibit greater variability in the timing of $\Delta^{14}C$ peak, likely revealing the influence of spatially variable upwelling on DIC $\Delta^{14}C$ in this region (e.g., Allen and Andrews, 2012; Haltuch et al., 2013). We find the halibut and rockfish records are in strong enough agreement to maintain the convention of tying peak $\Delta^{14}C$ to the year 1970 in northeast Pacific bamboo coral $\Delta^{14}C$ records (Roark et al., 2005). Nevertheless, in *Section 4.1*, we investigate the impact of assigning a later date to the $\Delta^{14}C$, and find that this does not affect the conclusions of this study.

Given the agreement in $\Delta^{14}C$ values among all six of the coral samples used in this study, the 1957 tie point for the other five coral $\Delta^{14}C$ records was tied to the $\Delta^{14}C$ value identified for the 1957 inflection point the of T1102 A12 bomb-spike record (Fig. 3a). For corals sampled at lower or slightly different resolutions through the initial rise in $\Delta^{14}C$, the location of the 1957 $\Delta^{14}C$ tie point ($\Delta^{14}C$ = -83.12‰) was identified by linearly interpolating between samples bracketing the $\Delta^{14}C$ value of -83.12‰ (Fig. 2). If the sample did not record the entire bomb-spike due to a hiatus or cessation in coral growth (Andrews et al., 2009), death, microbial degradation, or predation of the skeleton (i.e., samples T1101 A5 and T1101 A14), the date of the final $\Delta^{14}C$ point was extrapolated from the T1102 A12 reference $\Delta^{14}C$ curve (outermost T1101 A14 sample, $\Delta^{14}C$ = -29.51‰ tied to 1961.7; outermost T1101 A5 sample, $\Delta^{14}C$ = 3.6‰ tied to 1962.9; Fig. 2 e, f). Using measurements of gorgonin core radius during peeling, growth rates were determined between each of the tie points (Table 1). See more information on growth rate calculations in *Section 4.1*.

3.2 Statistical Analysis

Error associated with growth rate calculations was propagated from ±2 year uncertainty associated with 1957 (Roark et al., 2005; Hill et al., 2014). Slopes and y-intercepts were calculated to model the relationship between coral radius and growth rate data using a least squares linear regression. Uncertainty in these regressions were illustrated with 95% confidence bands. p-Values below 0.05 were considered statistically significant unless otherwise noted. Statistical analyses were performed using Prism 6 software for Mac (Version 7.0a, April 2016, GraphPad Software, Inc.)

4. RESULTS AND DISCUSSION

4.1 ^{14}C Bomb-spike derived extension rates: Evidence for non-linearity

All six gorgonin nodes recorded the expected increase in $\Delta^{14}C$ associated with the anthropogenic bomb spike (Fig. 2). A radial sampling resolution of ~0.5 mm and the precision of the reconnaissance method was sufficient to resolve the full $\Delta^{14}C$ curve (Fig. 2). All samples illustrated pre-bomb spike $\Delta^{14}C$ levels (~-120‰ to -90‰) and the initial $\Delta^{14}C$ onset (-90‰ to ~70‰). Four of the six coral profiles reach a $\Delta^{14}C$ maximum (~70‰) and subsequent decline to more recent $\Delta^{14}C$ values (~17-20‰; Fig. 2a-d). Two samples (T1101 A14 and T1101 A5) demonstrated only partial curves and did not reach the $\Delta^{14}C$ maximum (Fig. 2 e,f). However, all coral $\Delta^{14}C$ records closely matched each other as well as reference $\Delta^{14}C$ records from Gulf of Alaska halibut (*Hippoglossus stenolepis)* (Fig. 3; Piner and Wischniowski, 2004) and yelloweye rockfish *(Sebastes ruberrimus*) otoliths (Fig. 3; Kerr et al., 2004). Additionally, the $\Delta^{14}C$ excursion found in coral nodes used in this study is consistent with values reported in previous work (~-100‰ pre bomb spike to ~70‰ peak, Roark et al., 2005; Sherwood et al., 2009; Hill et al., 2014; Schiff et al., 2014). This suggests that the bomb spike is a reliable and reproducible phenomenon in bamboo corals from similar depths and locations (Fig. 2, 3a) and supports previous assertions that bamboo corals consume a surface-water derived food source that is reflected in their gorgonin node ^{14}C character (Griffin and Druffel, 1989; Roark et al., 2005; Hill et al., 2014).

While our $\Delta^{14}C$ profiles were generally consistent with previous studies, previous work on bamboo corals has only utilized one tie point in the bomb $\Delta^{14}C$ profile (1957) for radial extension rate calculations either due to lower sampling resolution, young coral age, or small nodal radii. In this study, our relatively high sampling resolution allowed us to identify the location of two chronological tie points in the $\Delta^{14}C$ curve (1957: initial $\Delta^{14}C$ rise; and 1970: $\Delta^{14}C$ maximum), which combined with the collection date (June, 2007) were used to calculate growth rates for two distinct periods (1957-1970 and 1970-2007.5) for four of the six corals. As mentioned above, two corals (T1101 A14 and T1101 A5), exhibited an initial $\Delta^{14}C$ rise linked to 1957, but never reached the 1970 $\Delta^{14}C$ maximum ($\Delta^{14}C$ = ~70‰). This may reflect coral death or cessation of growth before 1970, in agreement with written observations of T1101 A14 during sampling as "dead upon collection" (Table 1). Additionally, given the unlikelihood of finding a sample in corrosive California margin intermediate waters that has been dead for >40 years, another explanation for the lack of a complete bomb signal may be the removal of outer gorgonin material by predation or microbial degradation (Hill et al., 2014).

Using the chronological tie points determined for each sample, we calculated mean radial extension rates for the 1957-1970 and 1970-2007.5 time intervals ranging from ~10-220 μm/year (Table 2). Following

303 the approach used in previous studies, radial extension rate error was estimated by propagating a ±2 year
304 uncertainty associated with the onset of $\Delta^{14}C$ increase in Northern Hemisphere surface waters (Manning et al.,
305 1990; Kerr et al., 2004; Roark et al., 2005; Hill et al, 2014). Though uncertainty in the timing of the 1970 $\Delta^{14}C$
306 peak has not been previously reported, we also applied an uncertainty of ±2 years to the 1970 tie point. This
307 results in ~5-15% uncertainty on the calculated radial extension rates (or ±~1-30 μm/year), consistent with
308 previous work by Roark et al. (2005; Table 2). This ~5-15% uncertainty on the calculated radial extension rates
309 does not incorporate uncertainty associated with the width of the samples analyzed. We note, however, that
310 previously published calculations of bamboo coral radial extension rates using the $\Delta^{14}C$ bomb spike records
311 have not accounted for this additional source of uncertainty (e.g. Roark et al., 2005; Sherwood 2009; Hill et al.,
312 2014; Schiff et al., 2014). We estimate that the 0.3-0.8 mm width (average = 0.4 mm) of our peel samples
313 (Supplemental Table 1) reflect up to ~1-25 years' worth of growth (based on mean 1957-2007.5 radial
314 extension rates of 32-121 μm/year; mean = 5 years). Although this introduces additional uncertainty to our
315 calculated growth rate estimates, propagating the sample width as a source of error in the growth rate
316 calculation results in uncertainty estimates that are as large as the calculated radial extension rates. Thus, we
317 have followed the convention used in previous radial extension rate calculations of reporting only the
318 uncertainty associated with the timing of $\Delta^{14}C$ variations in surface water DIC (Roark et al., 2005; Sherwood et
319 al., 2009; Schiff et al., 2014; Hill et al., 2014).

320 Previous studies have determined a similarly large range of radial extension rates for bamboo corals:
321 54 – 93 μm/year for samples from the California margin (Hill et al., 2014), 20-75 μm/year for samples from
322 Newfoundland and Labrador (Sherwood and Edinger, 2009), 29-113 μm/year for samples from Tasmania
323 (Sherwood et al., 2009), 50-160 μm/year (Roark et al., 2005; Andrews et al., 2009) for samples from the Gulf
324 of Alaska, ~100 μm/year for bamboo corals from the Davidson Seamount, (Andrews et al., 2005), 12-78
325 μm/year based on calcite from samples collected in the western North Pacific (Farmer et al., 2015b), and 13-
326 114 μm/year for calcite samples from a wide range of depths (3-3950 m) in the Southern Hemisphere
327 (Thresher et al., 2016). Although our radial extension rate estimates (Table 2) for California margin bamboo
328 corals are largely consistent with the overall range of values determined in previous work, comparing the 1957-
329 1970 and 1970-2007.5 radial extension rates within each of our coral samples reveals a consistent decrease in
330 the rate of coral radial extension with coral age. Radial extension rates decreased by up to 90% between the

1957-1970 and 1970-2007.5 time periods (e.g. T1101 A17, Table 2). This trend is illustrated by the strong inverse relationship between coral nodal radius and radial extension rate ($r = -0.7$, $p = 0.03$; Fig. 4), which clearly demonstrates radial extension rate consistently decreases with increasing coral size.

Prior work has illustrated spatial heterogeneity in upwelling and thus, a delayed bomb radiocarbon peak in surface waters at some locations this region (see discussion in *Section 3.4*; Kerr et al., 2004; Piner and Wischniowski, 2004; Allen and Andrews, 2012; Haltuch et al., 2013). Therefore, we investigated whether uncertainty in the date assigned to the $\Delta^{14}C$ maximum affects the observed declines in radial extension rates in our corals. We recalculated the radial extension rates for our corals (as described in *Sections 3.4* and *4.1*) by assigning a date of 1980 to the $\Delta^{14}C$ maximum tie point instead of 1970 (Supplemental Table S2). Although the magnitude of the radial extension rate decline is reduced in this reanalysis (as would be expected), radial extension rates still declined by 9-77% between the 1957-1980 and 1980-2007.5 time intervals for three of four samples with complete $\Delta^{14}C$ curves (Supplemental Table S2). This indicates that it is unlikely that the observed growth rate decline is a result of poorly constrained uncertainty on the 1970 tie point alone. Instead, these results provide further evidence that the assumption of constant radial extension rates may result in uncertainty in coral age and poorly constrained chronologies. Additionally, these findings inspire further attempts to refine these chronologies using growth models.

4.2 Constructing a Nonlinear Growth Rate Model

The observed decline in radial extension rate with coral age and size suggests that bamboo coral chronologies that are based on an assumption of constant radial extension rate do not accurately represent coral growth. Hence, bomb-spike chronologies may be further refined by accounting for this growth rate nonlinearity. Here we explore whether the empirical relationship between coral radius and radial extension rate derived from our data can be used to construct chronologies for individual coral proxy records, or whether a simple model can be used to interpolate between chronological tie points.

4.2.1 Empirical relationship between radial extension rate and coral size

A clear inverse linear relationship is observed between node radius and radial extension rates determined for each of the two time periods for each California Margin coral (Fig. 4). A linear regression of these data and the associated 95% confidence interval yielded a statistically significant correlation between coral

radius (R) and radial extension rate (G; μm/year) given by equation (2). This equation will be referred to as the 'empirical relationship' and is plotted in Fig. 4.

$$G = (-26 \pm 10) * R + (202 \pm 47); r^2 = 0.44, p = 0.036 \quad (2)$$

Large variability in the size of the error bars for the calculated 1957-1970 radial extension rates resulted from the application of ±2 year uncertainty to both the 1957 and 1970 tie points over only a 13 year period (Table 2; Fig. 4). We note that some of the scatter of data apparent in Fig. 4 may be a result of the sources of uncertainty described above (e.g., uncertainty in the sampling width and timing of the $\Delta^{14}C$ tie points used in extension rate estimates). However, a statistically significant relationship between radial extension rate and coral radius is apparent despite these sources of uncertainty (Eqn. 2; Fig. 4).

To test whether the declining growth rate observed in the California margin coral samples is evident in bamboo corals from other regions, radiocarbon data from the basal nodes of three bamboo corals collected from Tasmanian seamounts (*Lepidisis spp.* and *Isidella spp.*) published by Sherwood et al. (2009) were reanalyzed as described in *Section 3.4* and *4.1* and included in our regression (Fig 4). Because the Sherwood et al. (2009) samples were collected south of Tasmania, the timing of the radiocarbon bomb spike inflection points was based on a New Zealand snapper otolith $\Delta^{14}C$ time series, which demonstrates the initial $\Delta^{14}C$ rise at 1957 and eventual $\Delta^{14}C$ peak at 1980 (Kalish et al., 1993; Sherwood et al., 2009). The samples were collected in 2007, providing a third chronological tie point. Although uncertainty in these tie points has not been discussed in the literature, we attributed a ±2-year uncertainty to the 1957 and 1980 data point to gauge uncertainty in comparison to California corals. Similar to corals from the California margin, all three Sherwood et al. (2009) samples demonstrated reduced radial extension rates with coral age and size (Table 2). That the radial extension rate data from the Sherwood et al. (2009) Tasmania samples generally agree with the magnitude and trends exhibited by our California margin corals supports the notion that skeletal growth dynamics may be similar across different bamboo coral taxa and regions of the ocean (Fig. 4).

Together, data from this study and Sherwood et al. (2009) substantiate preexisting notions that coral radial extension rate decreases with coral age and size (Grigg et al., 1974; Andrew et al., 2009; Noé and Dullo, 2006; Farmer et al., 2015b) and suggest that this phenomenon is not unique to bamboo corals from the California margin. Furthermore, these results support the development of nonlinear chronological models for bamboo coral taxa. A logical first-order approach to developing such non-linear age models is to simply utilize the empirical linear relationship calculated between radius and radial extension rate from the California margin

corals (Eqn. 2; Fig. 4). Accordingly, we applied Eqn. (2) to the $\Delta^{14}C$ records of each of the four live collected corals from this study to test whether the known features of the bomb spikes are accurately represented in a time series using this chronology method (Fig. 5). The resulting $\Delta^{14}C$ time series clearly show that the application of the empirical relationship fails to reproduce the expected $\Delta^{14}C$ curve in three of the four samples with complete $\Delta^{14}C$ records (Fig. 5). Offsets between the reconstructed and actual dates of the $\Delta^{14}C$ inflection points as large as 20+ years were observed (e.g. 1970, T1101 A7; Fig. 5), likely due to the large envelope of error in the empirical linear regression propagating through to the chronologies. This finding suggests that the empirical relationship alone is inadequate for chronology construction and that a more sophisticated approach to interpolating between chronological tie points is required.

4.2.2 Non-linear cross sectional area-based model

Although there is clearly a negative correlation between coral radius and radial extension, the uncertainty associated with the empirical relationship (Eqn. 2) is not sufficient for accurate chronology development, as is evident in Fig. 5. Hence, we explore the use of a growth rate model to understand as well as quantify changes in coral radial extension with coral age. One hypothesis to explain the observed decline of coral radial extension with age and size invokes a dynamic energy model. Based on energy allocation studies, organisms such as bamboo corals allocate a constant allotment of energy derived from limited food supply to somatic growth and devote any remaining energy resources to metabolic processes and reproduction (Kooijman, 2010). Based on this fundamental concept, we designed a growth rate model which assumes that a constant amount of gorgonin and calcitic skeleton is produced per unit time, despite variability in environmental conditions or food supply. Because this material is deposited around cylindrical coral nodes and internodes of increasing radius, the coral would extend at a decreasing rate radially as the coral circumference and area grow larger. Additionally, bamboo corals grow vertically over time, supporting a greater number of branches and polyps, which could result in reduced radial growth at the base (where our proxy records are derived) as more resources are allocated towards branch growth (Lasker et al., 2003; Noé et al., 2009; Watling et al., 2011). Here, we explore whether a simple mathematical model based on this concept can accurately reproduce the decline in radial extension rate with coral age and size illustrated by our data.

A simple mathematical model (hereafter referred to as the cross sectional area-based model) was employed to predict radial extension rates based on the concept that the change in cross-sectional area of both

418 gorgonin nodes and high Mg-calcite internodes deposited at the base of the coral is constant over time, with
419 the implication that an increasingly large coral will grow a lesser radial extent each year as it ages. In this model,
420 a cross section of a bamboo coral base is represented by a circle with an area (A, mm^2; Fig. 6a). Given that the
421 gorgonin nodes and internodes grow simultaneously, this model would represent the growth of both nodes as
422 well as the calcitic internodes. Assuming a constant amount (or cross sectional area) of calcite and gorgonin is
423 deposited around the circle each year (represented as dA/dt in the model), an area increasing at a constant rate
424 over time is represented by equations (3-4), where $\frac{d^2A}{dt^2} = 0$. Given the radial distances of the coral (in mm) at
425 1957 (R_{1957}) and 2007.5 ($R_{2007.5}$) provided by the $\Delta^{14}C$ data tie points, it is possible to calculate the increase in
426 area over that 50-year period to quantify dA/dt for each individual coral (Table 2). Equation (3) was used to
427 calculate dA/dt (mm^2/yr) from the radii at the 1957 and 2007.5 tie points (R_{1957} ; $R_{2007.5}$), where T is years of
428 coral growth, and A_T is the total area of the coral node (mm^2) deposited during that time.

429 $$dA/dt = (\pi(R_{2007.5})^2 - \pi(R_{1957})^2)/T \quad (3)$$

430 From this, a cross-sectional area-based growth rate can be used to assign a date to all points in a radial
431 dataset based on the radius of the coral at each point. For each radius (R) associated with the coral data
432 collection, the number of years (Δt) between R and the previous point (R_{-1}), dependent on sampling frequency,
433 can be determined by via equation (4), where $A_{(R-1)}$ represents the coral cross sectional area at the previous
434 radial increment.

435 $$\Delta t = (A_R - A_{(R-1)})/(dA/dt) \quad (4)$$

436 In practice, the radius (R) at each point in a proxy record and equations 5-7 would be used to derive a
437 Δt value between each point. From here, a chronology can be applied back from the outermost chronological
438 tie point, which would be the collection date for live-collected samples with complete $\Delta^{14}C$ bomb spikes.

439 Applying this area-based chronology method to the individual coral samples that exhibited the
440 complete $\Delta^{14}C$ bomb spike produced exponentially declining curves of radial extension rate versus node radius
441 (Fig. 7). These growth curves based on the area-based model reveal that model's growth rate predictions lie
442 within the 95% confidence interval of the linear regression of the experimental data, except at small coral radii
443 where rapid juvenile growth may occur (Fig. 7; Noé and Dullo, 2006; Farmer et al., 2015b). This overlap
444 between the area-based model outputs for each individual sample and the linear empirical relationship support
445 the concept that constant skeletal deposition may be a key mechanism for explaining the observed decline in

446 radial growth rates with coral age and radius. Applying an exponential fit to the experimental data yielded a
447 curve with a similar fit (r^2 = 0.5) as the linear empirical relationship (Eqn. 2), suggesting that an exponential
448 empirical relationship based on our dataset would not provide a much improved substitute for the model-based
449 radial growth prediction.

450 In order to validate the area-based model, we tested whether including the height dimension impacts
451 the growth rate predictions of the model. This was determined by using an alternative model (hereafter referred
452 to as the volume-based model) in which an individual gorgonin node is represented by a cylinder (Fig. 6b). This
453 approach requires adding a new term, 'h', to the area-based model to represent coral height. However, based on
454 observations while peeling samples for analysis, the geometry of an individual node can be slightly more
455 complex than is represented by a flat-top cylinder; our gorgonin nodes often demonstrated increasing height
456 with coral radius (Fig. 6b). To account for this, nodes were modeled with a slight increase in height with radius
457 (from h_i to h_f, in mm) using a quadratic equation (5), producing a ~15% increase in height over the coral
458 lifespan (e.g., an increase in height of 1.2 mm for a 10 mm diameter sample, roughly consistent with
459 observations of Δh while peeling).

460 $$h_r = (1/100)*R^2 + h_i \quad (5)$$

461 This h term was then added to equation (5) to predict a constant volume of gorgonin material
462 deposited per year ($\frac{d^2V}{dt^2} = 0$; Eqn. 6).

463 $$dV/dt = (\pi R_{2007}^2 - \pi R_{1957}^2)h/T \quad (6)$$

464 The same step-by-step procedure used in the area-based model was then applied to the volume-based
465 model to convert radius to time. Applying this volume-based chronology to sample T1101 A10, given $R_{2007.5}$ =
466 7.79 mm, R_{1957} = 3.828 mm, h_i = 8.0, and Δh = 15%, produced an exponentially declining curve of radial growth
467 rate versus node radius (Supplementary Fig. S1) that nearly mirrored the area-based growth rate prediction,
468 predicting slightly faster radial extension rates at small radii. Except for in the earliest growth phase of the coral,
469 this volume-based projection also fell largely within the 95% confidence interval of the empirical relationship
470 between radial extension and coral radius observed for our samples.

471 When considering the volume-based model results, it is critical to recognize that coral nodal height and
472 height change with radius were approximated via observations, rather than precisely measured as the nodes were
473 sampled. Testing the sensitivity of the volume-based model to changes in parameters such as height did reveal that

overall nodal height can impact growth rate predictions. Nevertheless, the similarity between the volume-based model and area-based model predictions of radial growth suggests that incorporating nodal height may not significantly impact chronologies (see comparison of area-based and volume-based models below). Hence, unless measurements of nodal height are purposefully taken during sampling, using a volume-based model may add unnecessary uncertainty to chronologies that may be more reliably constructed using the area-based model. In the following analyses we test the accuracy of the area-based model by applying this method to the bomb-spike profiles obtained from the four corals that recorded the complete bomb spike profile.

4.3 Application of Chronologies to Δ^{14}C Data

We tested the accuracy of the cross-sectional area-based model by applying this method to the $\Delta^{14}C$ profile from each of the corals. Since the key term in the model, dA/dt, can be calculated from two chronological tie points (1957 and 1970, 1950 and 2007.5, or 1970 and 2007.5), we can evaluate the accuracy of the model by examining the proximity of the date assigned to the $\Delta^{14}C$ maximum to 1970, which is not tied into the model. Thus, for each coral $\Delta^{14}C$ profile, we applied five different age models for comparison: (1) the cross sectional area model-based chronology tied to the 1957 and 1970 tie points (one dA/dt value, tied to the 1957 and 2007.5 tie points), (2) cross sectional area model-based chronology tied to three points (two dA/dt values calculated for 1957-1970 and 1970-2007.5), (3) the volume-based model chronology (one dV/dt value; 1957-2007.5), (4) the traditional linear interpolation method assuming constant radial extension between two tie points, and (5) the linear interpolation method assuming constant radial extension rate between three tie points (Table 2; Fig. 8). For each of the samples, the volume-based and area-based chronologies using two-tie points resulted in nearly identical $\Delta^{14}C$ time series (Supplementary Fig. S2, S3). This further demonstrates that incorporating nodal height into the growth rate model has minimal consequence on final chronologies, and that the simpler area-based model is sufficient for chronology construction.

The data plotted in Fig. 8 show that using two chronological tie points in the cross sectional area-based model approach substantially improves the accuracy of the traditional constant-growth rate model, which offsets the 1970 peak by 8-26 years in the samples with profiles extending to 2007 (Fig. 8 a-d). For samples T1101 A7 and T1102 A12, the two-tie-point area-based model improved the interpolation between the chronology tie points and captured the timing of the 1970 $\Delta^{14}C$ maxima accurately within ~3 years (1973; Fig. 8 a,b). Given the ±2 year uncertainty associated with the timing of the 1957 and 1970 tie points (*Section 4.1*), we

consider this ~3 year offset to be minimal and further validate the non-linear model as a method for reducing age model uncertainty associated with decreased radial extension rate with coral age/size.

While the non-linear models did improve age model accuracy from the 2-tie point linear interpolation method for the other two live-collected samples with complete $\Delta^{14}C$ bomb spikes, the area-based model still did not assign accurate dates to the 1970 $\Delta^{14}C$ maxima in sample T1101 A10 (1980; Fig. 8c), nor the branch sample, T1101 A17 (1994; Fig. 8d). Curiously, the branch sample, T1101 A17 had a small overall radius and slow increase in cross-sectional area with time (lower dA/dt) as compared to T1101 A7 and T1101 A10, even though T1101 A17 is on the same seamount and at a similar depth. A branch could grow at a different rate than the central stalk for a number of possible reasons, not limited to smaller polyp size or accessibility to food relative to other branches, which may be linked to local current flow. This suggests that the growth of bamboo coral branches may exhibit less predictable changes in growth with coral and that using basal node samples may result in stronger chronologies than branches when using this area-based model.

Although the offset for the T1101 A17 sample may be a result of different growth patterns for branches and basal sections of coral skeleton, the offset observed for sample T1101 A10 suggests that the bases of some corals also exhibit non-linear growth that is not fully represented by constant dA/dt in our model. This led us to investigate whether dA/dt changes with coral/age size as well. The analyses described above calculated dA/dt from the entire 1957-2007.5 interval, but comparing dA/dt calculated from both the 1957-1970 and 1970-2007.5 time windows for the four samples with complete $\Delta^{14}C$ records reveals that dA/dt also declines over the coral's lifespan. Calculations of dA/dt for each interval revealed notable declines between the 1957-1970 and 1970-2007.5 intervals for T1101 A7, T1101 A17, T1101 A10 and T1102 A12 (Table 2). The largest declines in dA/dt for samples T1101 A10 and T1101 A17 explain the area-based model's inability to place the $\Delta^{14}C$ peak at 1970 for these specimens. However, these observations are not surprising given that bamboo corals may not adhere to constant predictable growth patterns for several reasons. Firstly, these corals can exhibit asymmetric radial growth based on current direction and food availability (Noé and Dullo, 2006; Noé et al., 2009). This can result in variable growth rates from different radii of a single sample, defying our assumption of perfectly concentric deposition around a central axis. Additionally, studies have found evidence for major growth interruptions in bamboo corals based on patterns of ^{210}Pb decay (Andrews et al., 2009) as well as observations of dark seams in calcite that may result from the accumulation of surface-derived organic compounds when necrosis of the coenenchyme exposes the skeleton to sea water (Noé and Dullo, 2006; Noé

et al., 2009). Hence, while the assumption of constant dA/dt with coral age and size accurately represents non-linear radial extension in some coral chronologies, asymmetrical growth and the occurrence of additional abrupt growth interruptions as a coral matures could explain the observed decline in dA/dt between the 1957-1970 and 1970-2007.5 time periods. Sample T1101 A5 did exhibit obvious evidence of such organic seams based on visual inspection of adjoining basal calcite internodes in thin section (Supplemental Fig. 4). However, visual inspection of calcitic thin sections of the other five samples did not reveal obvious evidence of organic seams or growth hiatuses (Supplemental Fig. 4). Thus, it is unlikely that major hiatuses caused the observed declines in radial extension rate in our corals. This underscores the importance of (a) generating high-resolution $\Delta^{14}C$ bomb spike profiles that allow the age model (either linear or model-based) to be tied to three chronological tie points and (b) visually inspecting calcitic thin sections to identify major growth hiatuses.

The application of chronologies to T1101 A5 and T1101 A14 was more challenging given that neither record encompassed the entire bomb-$\Delta^{14}C$ profile (Fig. 8e, f), and the dA/dt values were calculated using an interpolated date for the outermost peel age (as described in section *4.1*). A similar procedure was necessary for the reanalyzed Sherwood et al. (2009) data, with a date interpolated for sample T.H17442 at 1979 and date interpolated for sample L4 at 1960 (Supplementary Figure S3b, c). It is more challenging to construct chronologies for samples such as these, which contain two or fewer reliable tie points. Additionally, it is difficult to determine why such records are incomplete and whether the organic node and calcite internode were affected similarly. For example, if the living tissue was removed, exposing the node and internode, there could be differential removal of calcite verses organic matter that could impact the synchronicity of the radiocarbon and proxy records from a coral, introducing even greater uncertainty to a chronology. Hence, these results highlight the importance of applying the bomb-spike chronology techniques to live-collected corals whose lifetime spans the entirety of the bomb spike era and whose skeleton has not been affected by predation or degradation.

These results illustrate that the cross sectional area-based model can generate more accurate chronologies than a traditional constant radial extension rate method. However, agreement between the three-tie point linear interpolation and cross-sectional area-based model chronologies clearly show that the identification of three chronological tie points between 1957 and the collection date results in the most reliable age models regardless of the interpolation method. Although the assumption that $\frac{d^2A}{dt^2} = 0$ may not always hold

perfectly, the model-based area approach represents an improved means of interpolating between tie points, as the modeled declines in growth rate (Fig. 7) are likely more realistic than the stepwise growth rate change that results from linear interpolations between points.

4.4 Biological Implications of the Growth Rate Nonlinearity

Given that the model described above appears to more accurately depict bamboo coral skeletal growth than traditional constant growth rate models, we can use this refined method to begin to explore trends in coral growth. With a suite of samples spanning ~800-1600 m depth along the California margin, we use our refined growth rate model to investigate whether depth (and thus, proximity to food source) influences skeletal growth. Notably, the $\Delta^{14}C$ curve of both T1101 A10 and T1101 A7, two corals collected from similar depths (<100 m apart) on the same seamount, exhibited similar dA/dt values (~3 mm^2/year). This could suggest that local environmental factors provide a control of the rate of skeletal material deposited each year. The calculated dA/dt value for sample T1101 A17 (819 m; 0.62 ± 0.2 mm^2/year; Tables 1, 2) was lower than those calculated for T1101 A10 or T1101 A7. Because particulate organic matter flux to depth decreases exponentially within the depth range of our samples (Lima et al., 2014), T1101 A17 would be expected to have a higher dA/dt value if food supply were the primary driver of skeletal growth rates. Hence, the difference in dA/dt values between samples of different depths and seamounts may reflect the unique growth-limiting environmental conditions in each coral location. The evident importance of environmental conditions is consistent with a previous suggestion that growth rates of Southern Hemisphere bamboo coral corals living in regions of high surface productivity or depths of maximum biomass density, are higher than those of samples from regions of reduced food supply (Thresher et al., 2016).

To further explore this concept, we compared the mean radial extension rate (calculated between 1957-2007.5) against depth for all six of our corals. A wide range of mean radial extension rates was observed 68 ± 32 μm/year (Fig. 9). The radial extension rates for four samples from the same location (T1101 A14, T1101 A5, T1101 A7, and T1101 A10, Pioneer Seamount) and similar depth (1028 ± 43 meters) exhibited a similar range (77 ± 33 μm/year; Fig. 9). However, based on our new evidence for growth rate non-linearity with coral age, a comparison of growth rates between corals likely necessitates a normalization for coral age. Thus, we used our area-based model to estimate each sample's radial extension rate when the coral was 30 years of age. For the same four Pioneer Seamount corals, modeled radial extension rates at 30 years of age were more

589 consistent (84 ± 11 μm/year; Fig. 9). The consistency in radial extension rates between samples at the same
590 age, depth, and location suggest that coral growth may be more consistent among individuals than previously
591 thought. This further supports the hypothesis underlying our model: bamboo corals follow a dynamic energy
592 budget, consistently allocating resources for growth regardless of variations in local environmental factors such
593 as depth or food supply (Kooijman, 2010). When the 30-year-old modeled growth rates for T1102 A12
594 (deeper, different seamount) and T1101 A17 (shallower depth) were included, growth rates remained consistent
595 (76 ± 19 μm/year). This suggests that while local conditions may affect the rate at which material is deposited
596 around an organic node each year (i.e., dA/dt), the conditions of our sampling locations may not have been
597 distinct enough to result in markedly differing radial extension rates between corals when normalizing for coral
598 age.
599
600 **5. CONCLUSIONS**
601 Applying accurate chronologies to proxy data is paramount in paleoclimate reconstructions. Hence,
602 uncertainty in radial growth has been a key obstacle to interpreting high resolution proxy data from these
603 uniquely positioned bamboo corals to understand climate variability at intermediate water depths. This study
604 provides evidence for declines in bamboo coral radial extension rate with coral age and size. Our work agrees
605 with previously sparse evidence suggesting that constant radial extension age models are inadequate for
606 accurate bamboo coral chronology construction. This study's findings also empower paleoceanographic efforts
607 with a means to refine chronologies using a simple mathematical model based on a constant increase in coral
608 cross sectional area with time ($\frac{d^2A}{dt^2} = 0$) due to prioritization of somatic growth in a coral's energy budget
609 allotments. Our results demonstrate that using a cross-sectional area-based age model consistently improves
610 upon the traditional linear interpolation method when only two age model tie points are available (e.g., 1957
611 and collection date), lending credibility to the model. Nevertheless, evidence from two corals suggest that the
612 assumption of constant dA/dt may not always perfectly represent commonly asymmetric bamboo coral
613 growth. Thus, incorporating a third tie point (e.g. 1970 $\Delta^{14}C$ peak) results in the most reliable age model
614 whether using the linear interpolation or the non-linear-modeling approach between the three tie points. These
615 results suggest that considerable uncertainty remains when assigning chronologies to the pre-bomb era.
616 Further, age estimates of bamboo corals may have been overestimated when constant radial extension rate was

assumed. This methodology provides a more realistic means of interpolating growth rate between tie points, particularly when only two tie points can be identified in a coral's $\Delta^{14}C$ record, and avoids the need to employ an unrealistic 'step function' in using the radial extension rates calculated for the 1957-1970 and 1970-2007.5 intervals. Meanwhile, the finding that corals of similar depth and location exhibit similar age-normalized growth rates suggests growth limitation by local environmental conditions. Continued research on bamboo coral growth nonlinearity and identification of additional pre-bomb spike age model tie points will continue to improve the accuracy of age estimates and chronologies for samples with significant growth before 1957 and extend the reliability of these unique paleoarchives back in time.

7. ACKNOWLEDGEMENTS

The authors wish to thank the many individuals who contributed to this research effort, including scientists at NOSAMS who made the radiocarbon analyses process as smooth and easy as possible, Jamie Ptacek, and the Earth and Oceanographic Science students and faculty at Bowdoin College for valuable feedback. The authors would also like to thank Dr. Owen Sherwood (CU-Boulder) for sharing data that greatly contributed to this paper. The review provided by Les Watling contributed to the biological concepts included in the discussion; and two anonymous reviewers greatly improved the quality of this manuscript. This research was made possible by National Science Foundation Award #1420984 to M. LaVigne and a Clare Boothe Luce Fellowship to M. Frenkel. M. Frenkel completed this work as an undergraduate research student in M. LaVigne's laboratory at Bowdoin College.

Coral data are are available as supplementary material and from the World Data Center for Paleoclimatology, 325 Broadway, Boulder, Colorado; ftp://ftp.ncdc.noaa.gov/pub/data/paleo/coral/xxxx/; email: paleo@noaa.gov.

8. REFERENCES

Allen, L.G and A. Andrews (2012), Bomb Radiocarbon Dating and Estimated Longevity of Giant Sea Bass (*Stereolepis gigas*), *Bulletin of the Southern California Academy of Sciences,* 111(1), 1-14.

Andrews, A.H., E.E. Cordes, M.M. Mahoney, K. Munk, K.H. Coale, G.M. Cailliet and J. Heifetz (2002), Age, growth and radiometric age validation of a deep-sea habitat-forming gorgonian (*Primnoa resedaeformis)* from the Gulf of Alaska, *Hydrobiologia,* 471, 101-110, doi: 10.1023/A:1016501320206.

647 Andrews, A.H., G.M. Cailliet, L.A. Kerr, K.H. Coale, C. Lundstrom and A.P. DeVogelaere (2005),
648 Investigations of age and growth for three species of deep-sea coral from the Davidson Seamount off
649 central California, in *Cold-water Corals and Ecosystems*, edited by Freiwald, A. and Roberts, J.M, Springer-
650 Verlag, Berlin, 965-982.
651 Andrews, A.H., R.P. Stone, C.C. Lundstrom and A.P. DeVogelaere (2009), Growth rate and age determination
652 of bamboo corals from the northeastern Pacific Ocean using refined ^{210}Pb dating, *Marine Ecology Press*
653 *Series,* 397, 173-185, doi: 10.3354/meps08193.
654 Bijma, J., H.O. Portner, C. Yessen, and A.D. Rogers (2013), Climate change and the oceans – What does the
655 future hold?, *Marine Pollution Bulletin,* 2(74), 1-11, doi.org/10.1016/j.marpolbul.2013.07.022.
656 Burke, A., L.F. Robinson, A.P. McNichol, W.J. Jenkins, K.M. Scanlon and D.S. Gerlach (2010),
657 Reconnaissance dating: A new radiocarbon method applied to assessing the temporal distribution of
658 Southern Ocean deep-sea corals, *Deep Sea Research Part 1: Oceanographic Research Papers*, 57(11),1510-1520,
659 doi: 10.1016/j.dsr.2010.07.010.
660 Cheng, H., J. Adkins, R.L. Edwards and E.A. Boyle (2000), U-Th dating of deep-sea corals, *Geochemica et*
661 *Cosmochimica Acta,* 64(14), 2401-2416, doi: 10.1015/S0016-7037(99)00422-6.
662 Cobb, K.M., C.D. Charles, H. Cheng, M. Kastner and R.L Edwards (2003), U/Th-dating living and young
663 fossil corals from the central tropical Pacific, *Earth and Planetary Science Letters*, 210, 91-103,
664 doi:10.1016/S0012-821X(03)00138-9.
665 Druffel, E.R.M., L.L. King, R.A. Belastock and K.O. Buesseler (1990), Growth rate of deep-sea coral using
666 ^{210}Pb and other isotopes, *Geochimica et Cosmochimica Acta,* 54(5)*,* 1493-1499, doi: 10.1016/0016-
667 7037(90)90174-J.
668 Edinger, E.N., O.A. Sherwood, D.J.W. Piper, V.E. Wareham, K.D. Baker, K.D. Gilkinson and D.B. Scott
669 (2011), Geological features supporting deep-sea coral habitat in Atlantic Canada, Continental Shelf
670 Research, 31, S69-S84, doi: 10.1016/j.csr.2010.07.004.
671 Fabricius, K. (2011), Octocorallia, in *Encyclopedia of Modern Coral Reefs: Structure, Form and Process*, Encyclopedia of
672 Earth Sciences, edited by D. Hopley, Springer, Dordrecht, The Netherlands.
673 Farmer, J., B. Hönisch, J. Robinson and T.M. Hill (2015a), Effects of seawater-pH and biomineralization the
674 boron isotopic composition of deep-sea bamboo corals, *Geochminica et Cosmochimica Acta,* 155, 86-106,
675 doi.org/10.1016/j.gca.2015.01.018.
676 Farmer, J., L. Robinson and B. Hönisch (2015b), Growth rate determinations from radiocarbon in bamboo
677 corals (genus Keratoisis), *Deep-Sea Research I*, 105, 26-40, doi:10.1016/j.dsr.2015.08.004.
678 France, S.C. (2007), Genetic analysis of bamboo corals (Cnidaria: Octocorallia: Isididae): does lack of colony
679 branching distinguish Lepidisis from Keratoisis? *Bulletin of Marine Science,* 81, 323–333.
680 Grant, R. (1976), The marine fauna of New Zealand: Isididae (Octocorallia: Gogonacea) from New Zealand
681 and the Antarctic, *New Zealand Oceanographic Institute Memoir*, 66*,* 5-54.
682 Griffin, S. and E.R.M. Druffel (1989), Source of Carbon to Deep-Sea Corals, *Radiocarbon*, 31(3), 533-543,
683 doi: doi.org/10.1017/S0033822200012121.
684 Grigg, R.W. (1974), Growth Rings: Annual Periodicity in Two Gorgonin Corals, *Ecology*, 55*,* 876-881.

685 Haltuch, M., Hamel, O.S., Piner, K.R., McDonald, P., Kastelle, C.R., Field, J.C. (2013), A California Current
686 bomb radiocarbon reference chronology and petrale sole (*Eopsetta jordani*) age validation, *Canadian Journal*
687 *of Fisheries and Aquatic Sciences,* 70, 22-31, doi: 10.1139/cjfas-2011-0504.
688 Hill, T. M., H.J. Spero, T. Guilderson, M. LaVigne, D. Clague, S. Macalello, S and N. Jang (2011), Temperature
689 and vital effect controls on bamboo coral (*Isididae*) isotope geochemistry: A test of the "lines method,"
690 *Geochemistry, Geophysics, Geosystems,* 12(4), Q04008, doi: 10.1029/2010GC003443.
691 Hill, T. M., M. LaVigne, H. J. Spero, T. Guilderson, B. Gaylord, and D. Clague (2012), Variations in seawater
692 Sr/Ca recorded in deep-sea bamboo corals, *Paleoceanography*, 27, PA3202, doi:10.1029/2011PA002260.
693 Hill, T. M., C.R. Myrvold, H. Spero and T. Guilderson (2014), Evidence for benthic-pelagic food web coupling
694 and carbon export from California margin bamboo coral archives, *Biogeosciences*, 11, 3845-3854,
695 doi:10.5194/bg-11-3845-2014.
696 Kalish, J.M., J.M. Johnston, D.C. Smith, A.K. Morison and S.G. Robertson (1993), Use of the bomb
697 radiocarbon chronometer for age validation in the blue grenadier *Macruronus novaezelandiae,* Marine
698 Biology, 128, 557-563, doi:10.1007/s002270050121.
699 Keeling, R. F., A. Kortzinger and N. Gruber. (2010), Ocean Deoxygenation in a Warming World, *Annual Review*
700 *of Marine Science, 2,* 199-229, doi:10.1146/annurev.marine.010908.163855.
701 Kerr, L.A., A.H. Andrews, B.R. Frantz, K.H. Coale, T.A. Brown and G.M Calliet (2004), Radiocarbon in
702 otoliths of yelloweye rockfish (*Sebastes ruberrimus)*: a reference time series for the coastal waters of
703 southeast Alaska, *Canadian Journal of Fisheries and Aquatic Science,* 61*,* 443-451, doi: 10.1139/F04-009.
704 Kerr, L. A., A.H. Andrews, K. Munk, G.M. Cailliet, K.H. Coale, T.A. Brown and B.R. Frantz (2005), Age
705 validation of quillback rockfish (*Sebastes malinger)* using bomb radiocarbon, *Fishery Bulletin,* 103, 97-107.
706 Kimball, J.B., R.B. Dunbar and T.P. Guilderson (2014), Oxygen and carbon isotope fractionation in calcitic
707 deep-sea corals: Implications for paleotemperature reconstruction, *Chemical Geology*, 381*,* 223-233, doi:
708 10.1016/j.chemgeo.2014.05.008.
709 Kooijman, S.A.LM. (2010), *Summary of concepts of Dynamic Energy Budget theory for metabolic organisation*, 2nd ed., pp.
710 70, Cambridge University Press, Cambridge, UK.
711 Lacharité, M. and A. Metaxas (2013), Early Life History of Deep-Water Gorgonian Corals May Limit Their
712 Abundance, *PLoS ONE,* 8(6), e65394, doi:10.1371/journal.pone.0065394.
713 Lasker, H.R., M.L. Boller, J. Castanaro and J.A. Sanchez (2003), Determinate Growth and Modularity in
714 Gorgonian Octocoral, *The Biological Bulletin*, 205(3), 319-330, doi: 10.2307/1543295.
715 LaVigne, M., T.M. Hill, H.J. Spero and T.P. Guilderson (2011), Bamboo coral Ba/Ca: Calibration of a new
716 deep ocean refractory nutrient proxy*, Earth and Planetary Science Letters,* 312, 506-515,
717 doi:10.1016/j.epsl.2011.10.013.
718 Lima, I.D., P.J. Lam and S.C. Doney (2014), Dynamics of particulate organic carbon flux in a global ocean
719 model, *Biogeosciences*, 11, 1177-1198, doi:10.5194/bg-11-1177-2014.
720 Longworth, B.E., K.F. von Reden, P. Long and M.L. Roberts (2015), A high output, large acceptance injector
721 for the NOSAMS Tandetron AMS System, *Nuclear Instruments and Methods in Physics Research B,* 361*,* 211-
722 2016, doi.org/10.1016/j.nimb.2015.04.005.

723 Manning, M.R., D.C. Lower, W.H. Melhuish, R.J. Sparks, G. Wallace, C.A.M. Brenninkmeijer and R.C. McGill
724 (1990), The use of radiocarbon measurements in atmospheric studies, *Radiocarbon,* 32*,* 37-58.
725 Noé, S.U., and W.C. Dullo (2006), Skeletal morphogenesis and growth mode of modern and fossil deep-water
726 isidid gorgonians (Octocorallia) in the West Pacific (New Zealand and Sea of Okhotsk), *Coral Reefs,* 25,
727 303-320, doi:10.1007/s00338-006-0095-8.
728 Noé, S.U., L. Lembke-Jene and W.C. Dullo (2009), Varying growth rates in bamboo corals: schlerochronology
729 and radiocarbon dating of a mid-Holocene deep-water gorgonin skeleton (*Keratoisis* sp.: Octocorallia)
730 from Chatham Rise (New Zealand), *Facies*, 54*,* 151-166. doi: 10.1007/s10347-007-0129-x.
731 Olsson, I.U. (1970), The use of Oxalic acid as a Standard, in *Radiocarbon Variations and Absolute Chronology,* Nobel
732 Symposium, 12th Proc., edited by I.U. Olsson, John Wiley & Sons, New York, p. 17.
733 Piner, K.R. and S.G. Wischniowski, (2004), Pacific halibut chronology of bomb radiocarbon in otoliths from
734 1944 to 1981 and a validation of ageing methods, *Journal of Fish Biology,* 64, 1060-1071,
735 doi:10.1111/j.1095-8649.2004.00371.
736 Prouty, N.G., E.B. Roark, A. Andrews, L. Robinson, T. Hill, O. Sherwood, B. Williams, T. Guilderson and S.
737 Fallon (2015), Age, Growth, and Paleoclimate Studies of Deep Sea Corals, in *The State of Deep-Sea Coral*
738 *and Sponge Ecosystems of the United States*, edited by Hourigan, T.F., Etnoyer, P.J., and Cairns, S.D., NOAA
739 Technical Memorandum X, NOAA, Silver Spring, 10-1-10-21.
740 Roark, B., T. Guilderson, S. Flood-Page and R. Dunbar (2005), Radiocarbon-based ages and growth rates of
741 bamboo corals from the Gulf of Alaska, *Geophysical Research Letters*, 32, L04606,
742 doi:10.1029/2004GL021919.
743 Ryan, W.B.F., S.M. Carbotte, J.O. Coplan, S. O'Hara, A. Melkonian, R. Arko, R.A. Weissel, V. Ferrini, A.
744 Goodwillie, F. Nitsche, J. Bonczkowski, and R. Zemsky (2009), Global Multi-Resolution Topography
745 synthesis, *Geochem. Geophys. Geosyst.*, 10, Q03014, doi:10.1029/2008GC002332.
746 Saenger, C. and J.M. Watkins (2016), A refined method for calculating paleotemperatures from linear
747 correlations in bamboo coral carbon and oxygen isotopes, *Paleoceanography,* 31(6), 789-799, doi:
748 10.1002/2016PA002931.
749 Schiff, T. J., F.C. Batista, O.A. Sherwood, T.P. Guilderson, T.M. Hill, A.C. Ravelo, K.W. McMahon and M.D.
750 McCarthy (2014), Compound specific amino acid $\delta^{13}C$ patterns in deep-sea proteinaceous coral:
751 Implications for reconstructing detailed $\delta^{13}C$ records of exported primary production, *Marine Chemistry,*
752 166, 82-91, doi.org/10.1016/j.marchem.2014.09.008.
753 Sherwood, O.A., Scott, D.N., and Risk, M.J. (2006), Late Holocene radiocarbon and aspartic acid racemization
754 dating of deep-sea octocorals, *Geochimica et Cosmochimica Acta, 70*(11), 2806-2814,
755 doi:10.1016/j.gca.2006.03.011.
756 Sherwood, O.W. and E. Edinger (2009), Age and growth rates of some deep-sea gorgonian and antipatharian
757 corals of Newfoundland and Labrador, *Canadian Journal of Fisheries and Aquatic Sciences,* 66*,* 142-152,
758 doi:10.1139/F08-195.

759 Sherwood, O.W., R.E. Thresher, S.J. Fallon, D.M. Davies and T.W. Trull (2009), Mutli-century time-series of
760 15N and 14C in bamboo corals from deep Tasmanian seamounts: evidence from table oceanographic
761 conditions, *Marine Ecology Progress Serie*s, 397, 209-218, doi: 10.3354/meps08166.
762 Sinclair, D.J., B. Williams, G.Allard, B. Ghaleb, S. Fallon, S.W. Ross and M. Risk (2011), Reproducibility of
763 trace element profiles in specimen of deep-water bamboo coral *Keratoisis sp., Geochimica et Cosmochimica*
764 *Acta,* 75, 5101-5121, doi:10.1016/j.gca.2011.05.012.
765 Stramma, L., S. Schmidtko, L.A. Levin and G.C. Johnson (2010), Ocean oxygen minima expansions and their
766 biological impacts, *Deep Sea Research I*, 1-9, doi:10.1016/j.dsr.2010.01.005.
767 Stuiver, M. and H.A. Polach (1977), Discussion: Reporting of ^{14}C data. *Radiocarbon*, 19(355-363).
768 Thresher, R., S.R. Rintoul, J.A. Koslow, C. Weidman, J. Adkins and C. Proctor (2004), Oceanic evidence of
769 climate change in southern Australia over the last three countries, *Geophysical Research Letters,* 31(7),
770 L07212 1-4, doi:10.1029/2003GL018869.
771 Thresher, R. (2009), Environmental and composition correlates of growth rate in deep-water bamboo coral,
772 *Marine Ecology Progress Series,* 397*,* 187-196, doi: 10.3354/meps08245.
773 Thresher, R.E., C.M. MacRae, N.C. Wilson and S. Fallon (2009), Feasibility of age determination of deep-water
774 bamboo corals (Gorgonacea; Isididae) from annual cycles in skeletal composition, *Deep-Sea Research I*, 56*,*
775 442-449, doi:10.1016/j.dsr.2008.10.003.
776 Thresher, R.E., S.J. Fallon and A.T. Townsend (2016), A "core-top" screen for trace element proxies of
777 environmental condition and growth rates in calcite skeletons of bamboo corals (Isididae), *Geochimica et*
778 *Cosmochimica Acta,* 193*,* 75-99, doi: 10.1016/j.gca.2016.07.033.
779 von Reden, K.F., J.C. Donoghue, K.L. Elder, A.R. Gagnon, D.S. Gerlach, V.S. Griffin, R.J. Healy, P. Long,
780 A.P. McNichol, D. Percy, M.L. Roberts and R.J. Schneider (2004), Plans for expanded ^{14}C analyses at the
781 NOSAMS facility – A status and progress report, *Nuclear Instruments and Methods in Physics Research B,* 223-
782 224*,* 50-54, doi:10.1016/j.nimb.2004.04.014.
783 Watling, L., S.C. France, E. Pante and A. Simpson. (2011), Biology of Deep-Water Octocorals, in *Advances in*
784 *Marine Biology,* edited by M. Lesser, vol. 60, Elsevier, Philadelphia, PA.
785 Wong, C.S., F.A. Whitney, D.W. Crawford, K. Iseki, R.J. Matear, W.K. Johnson, J.S. Page and D. Timothy
786 (1999), Seasonal and interannual variability in particle fluxes of carbon, nitrogen and silicon from time
787 series of sediment traps at Ocean Station P, 1982–1993: relationship to changes in subarctic primary
788 productivity, *Deep Sea Research Part II: Topical Studies in Oceanography,* 46(11-12), 2735-2760,
789 doi:10.1016/S0967-0645(99)00082-X.
790 Xu, X., S.E. Trumbore, S. Zheng, J.R. Southon, K.E. Mcduffee and M. Luttgen (2007), Modifying a sealed tube
791 zinc reduction method for preparation of AMS graphite targets, *Nuclear Instruments and Methods in Physics*
792 *Research B,* 259*,* 320-329, doi: 10.1016/j.nimb.2007.01.175.
793
794
795

Figures:

Figure 1. The geographic locations of coral samples used in this study ((Pioneer Seamount and Davidson Seamounts; red dots), plotted on a map of bathymetry generated using GeoMappApp (http://www.geomapapp.org; Ryan et al., 2009).

Figure 2. Gorgonin node $\Delta^{14}C$ plotted with distance from the coral core for samples (a) T1101 A17, (b) T1102 A12, (c) T1101 A7, (d) T1101 A10, (e) T1101 A14, and (f) T1101 A5. Uncertainties in $\Delta^{14}C$ measurements (~ 0.01-0.40 ‰) are smaller than the symbols. Chronological tie points indicated with dashed line.

Figure 3. (a) Radiocarbon ($\Delta^{14}C$) time series for all coral samples analyzed. Dotted lines indicate locations of chronological tie points (1957, 1970, and 2007.5) assigned to $\Delta^{14}C$ records with linear interpolation between tie points (Table 1). The 1957-1970 radial extension rate was assigned to data points prior to 1957. (b) Overlay of radiocarbon time series for coral T1101 A10 shown in (a) (red triangle), Gulf of Alaska yelloweye rockfish otolith data (grey circles) from Kerr et al. (2004) and Gulf of Alaska Pacific halibut otolith data (blue diamonds) from Piner and Wischniowski (2004).

Figure 4. Radial extension rate versus coral nodal radius (using the radial distance at the 1957 and 1970 tie points for the 1957-1970 and 1970-2007.5 rates, respectively) for all samples in this study (blue circles) including reanalyzed data from Sherwood et al. (2009; red triangles). Note that the error bars for some samples are smaller than their associated data point. Black line represents best-fit linear regression through California margin coral data points (Eqn. 2), with a 95% confidence interval (dashed curve).

Figure 5. Time series of $\Delta^{14}C$ records for all live-collected corals with complete $\Delta^{14}C$ bomb spikes based on application of the empirical relationship (Eqn. 2) plotted with the Kerr et al. (2004) yelloweye rockfish otolith record. See *Section 4.1.*

Figure 6. (a) Schematic of cross sectional area model. (b) Model of a single gorgonin node used in volume-based model where height (h) increases with coral radius (R) from the initial height at the core of the node (h_i) to its final height (h_f). In the volume-based model, $(h_f - h_i)/h_i = 0.15$ for all samples, for consistency.

Figure 7. Radial extension rate (μm/year) versus coral radius (mm) for California margin data points shown in Fig. 4 (black circles) plotted with the empirical relationship (Eqn. 2; black dotted curve with grey 95% confidence interval) and area-based model predictions for samples T1101 A10 (red), T1101 A17 (blue), T1101 A7 (orange), and T1102 A12 (green).

Figure 8. Reconstructed time series of $\Delta^{14}C$ (‰) for (a) T1101 A7, (b) T1102 A12, (c) T1101 A10, (d) T1101 A17 (e) T1101 A5 and (f) T1101 A14 based on a linear interpolation between tie points at 1957, 1970 and 2007.5 (filled dark blue squares, solid curve), a linear interpolation between 1957 and 2007.5 tie points (unfilled light blue squares, dashed curve), and the application of the area-based model using dA/dt for the 1957-2007.5 interval (orange unfilled circles, dashed curve), and the area-based model using distinct dA/dt values for the 1957-1970 and 1970-2007.5 intervals (filled red circles, solid curve). Otolith $\Delta^{14}C$ records (Kerr et al., 2004) are represented by grey dots and the 1970 tie point is shown by the black dashed line.

Figure 9. Radial extension rate (μm/yr) as a function of coral depth for samples from the Davidson Seamount (triangles) and Pioneer Seamount (circles) based on the average growth rate from 1957 – 2007.5 (red) and from the growth rate predicted at age 30 years determined from the application of the area-based model chronology to each coral sample (blue).

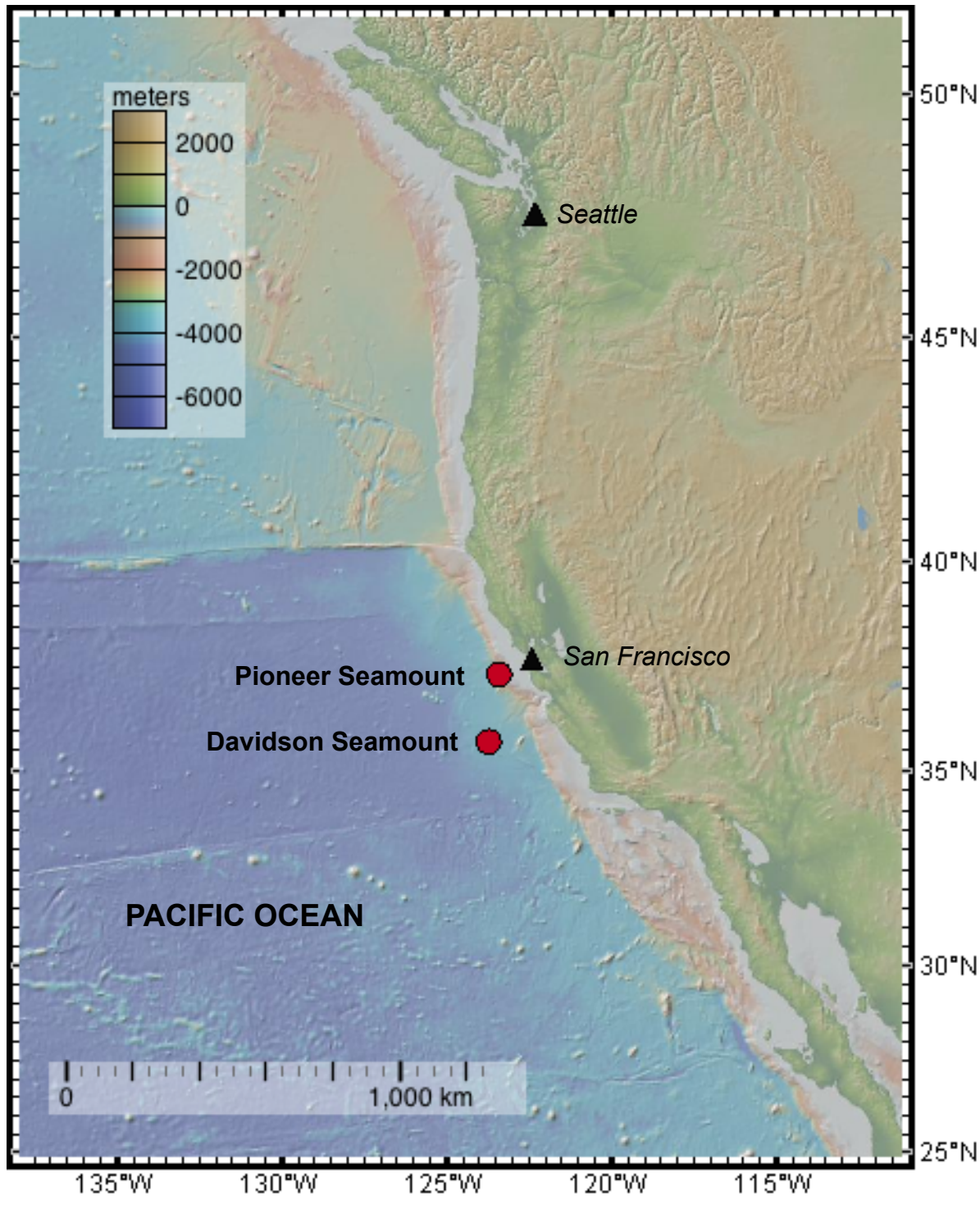
meters
2000
0
-2000
-4000
-6000
Seattle
San Francisco
Pioneer Seamount
Davidson Seamount
PACIFIC OCEAN
0
1,000 km
50°N
45°N
40°N
35°N
30°N
25°N
135°W
130°W
125°W
120°W
115°W

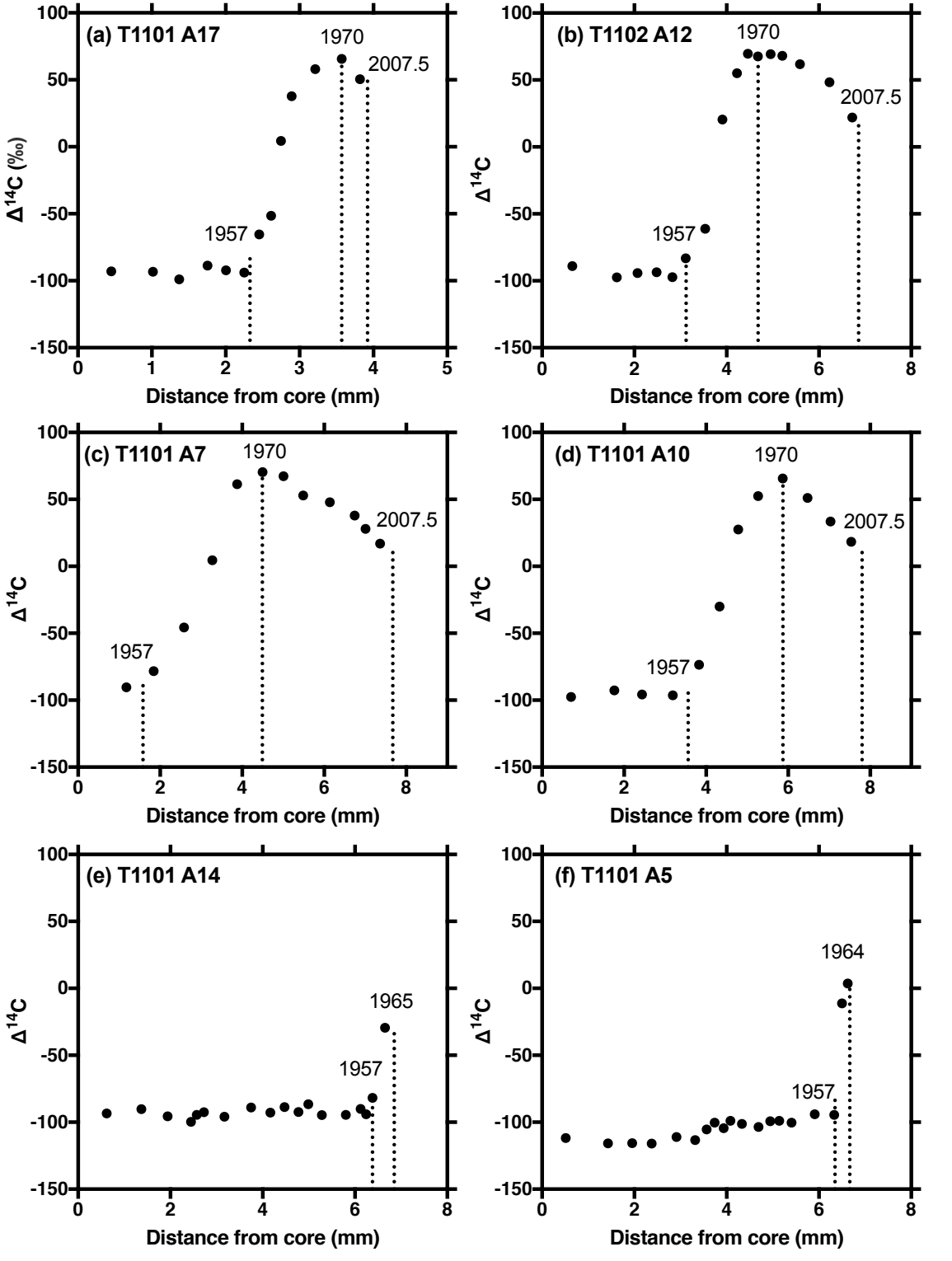
(a) T1101 A17
1970
2007.5
1957
Δ14C (‰)
Distance from core (mm)
(b) T1102 A12
1970
2007.5
1957
Δ14C
Distance from core (mm)
(c) T1101 A7
1970
2007.5
1957
Δ14C
Distance from core (mm)
(d) T1101 A10
1970
2007.5
1957
Δ14C
Distance from core (mm)
(e) T1101 A14
1965
1957
Δ14C
Distance from core (mm)
(f) T1101 A5
1964
1957
Δ14C
Distance from core (mm)

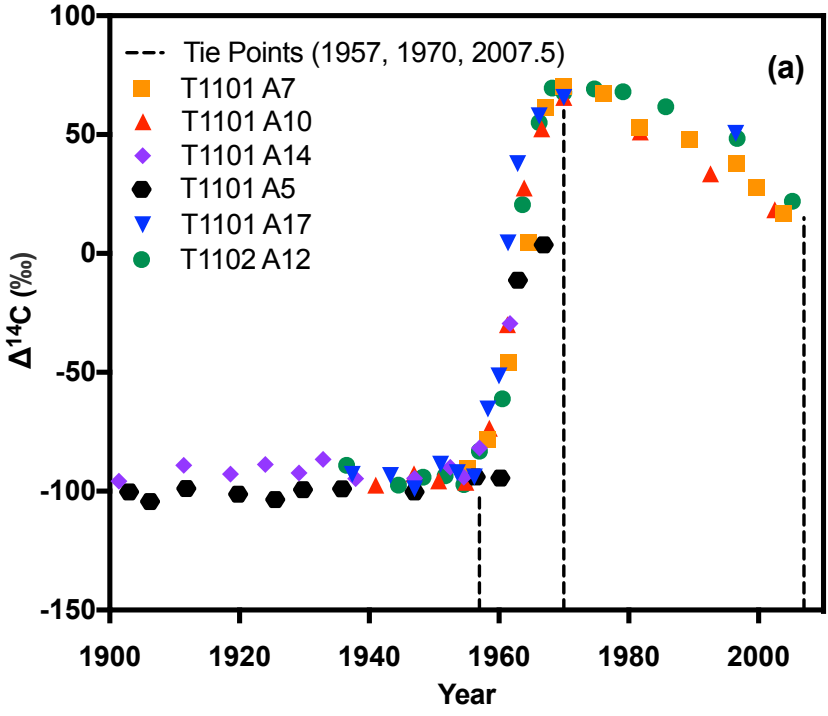
Tie Points (1957, 1970, 2007.5)
T1101 A7
T1101 A10
T1101 A14
T1101 A5
T1101 A17
T1102 A12
(a)
Δ14C (‰)
Year
100
50
0
-50
-100
-150
1900
1920
1940
1960
1980
2000

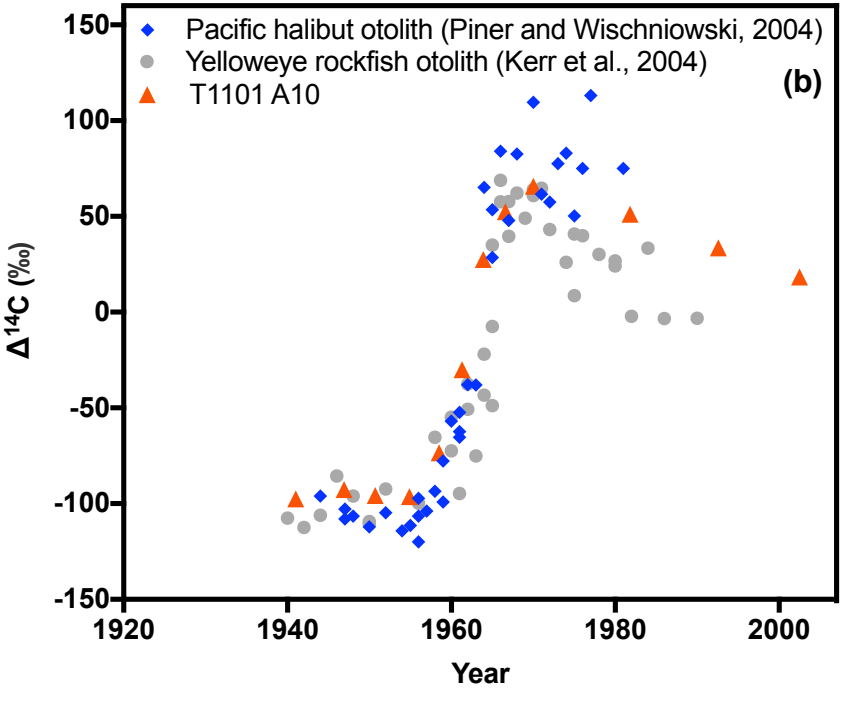
Pacific halibut otolith (Piner and Wischniowski, 2004)
Yelloweye rockfish otolith (Kerr et al., 2004)
T1101 A10
(b)
Δ14C (‰)
Year
150
100
50
0
-50
-100
-150
1920
1940
1960
1980
2000

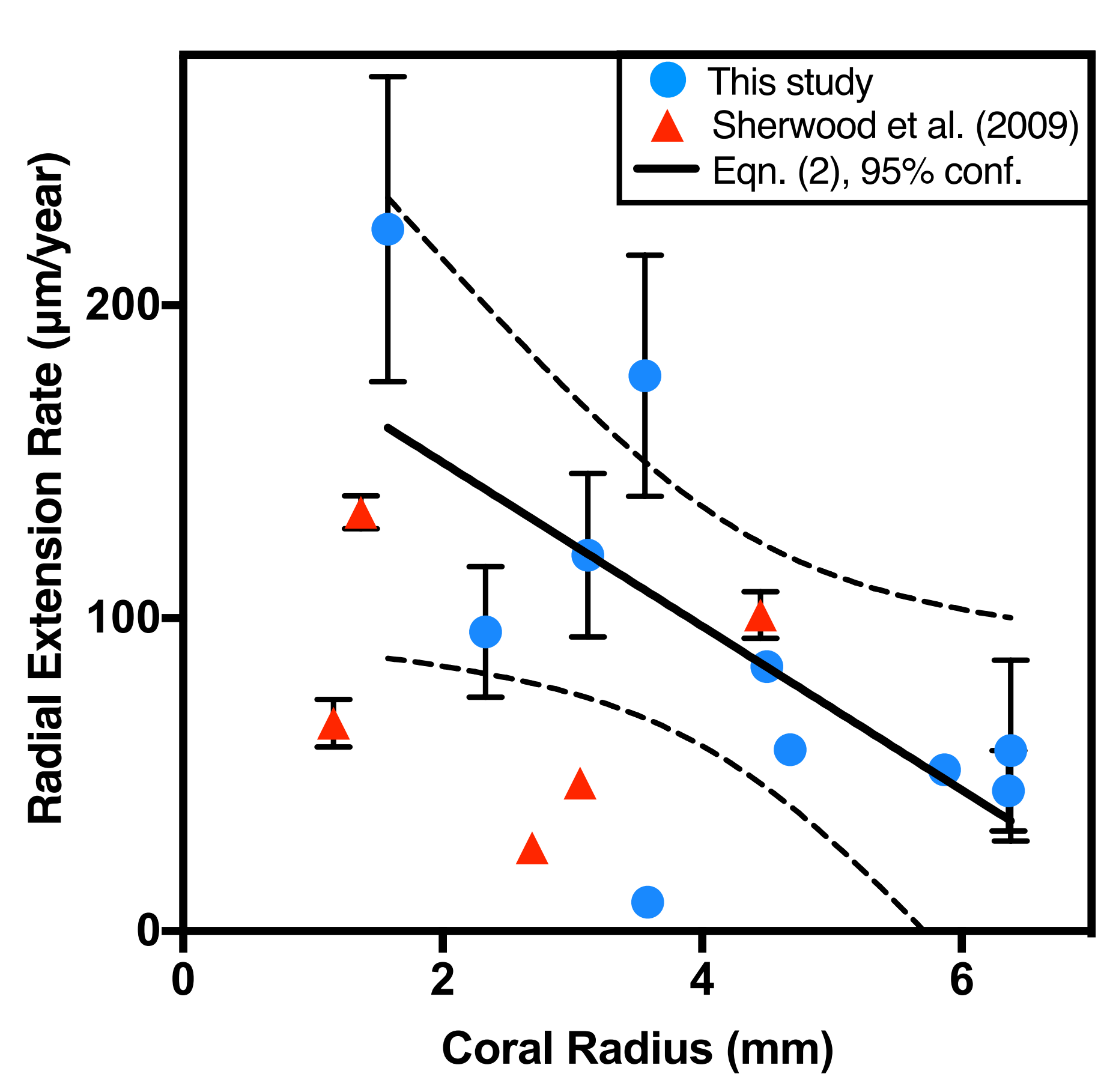
This study
Sherwood et al. (2009)
Eqn. (2), 95% conf.
Radial Extension Rate (µm/year)
200
100
0
0
2
4
6
Coral Radius (mm)

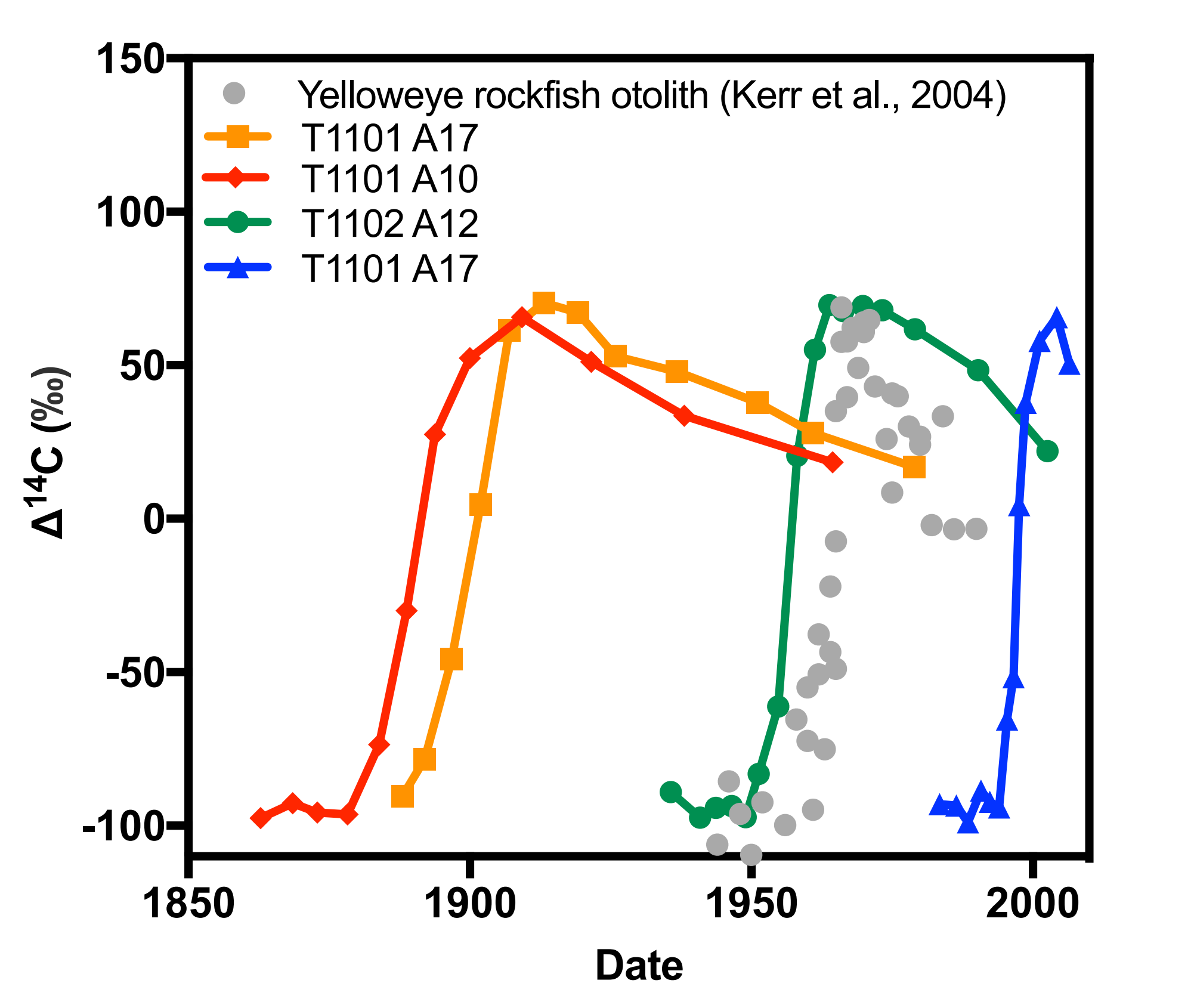
Yelloweye rockfish otolith (Kerr et al., 2004)
T1101 A17
T1101 A10
T1102 A12
T1101 A17
150
100
50
0
-50
-100
Δ14C (‰)
1850
1900
1950
2000
Date

(a)

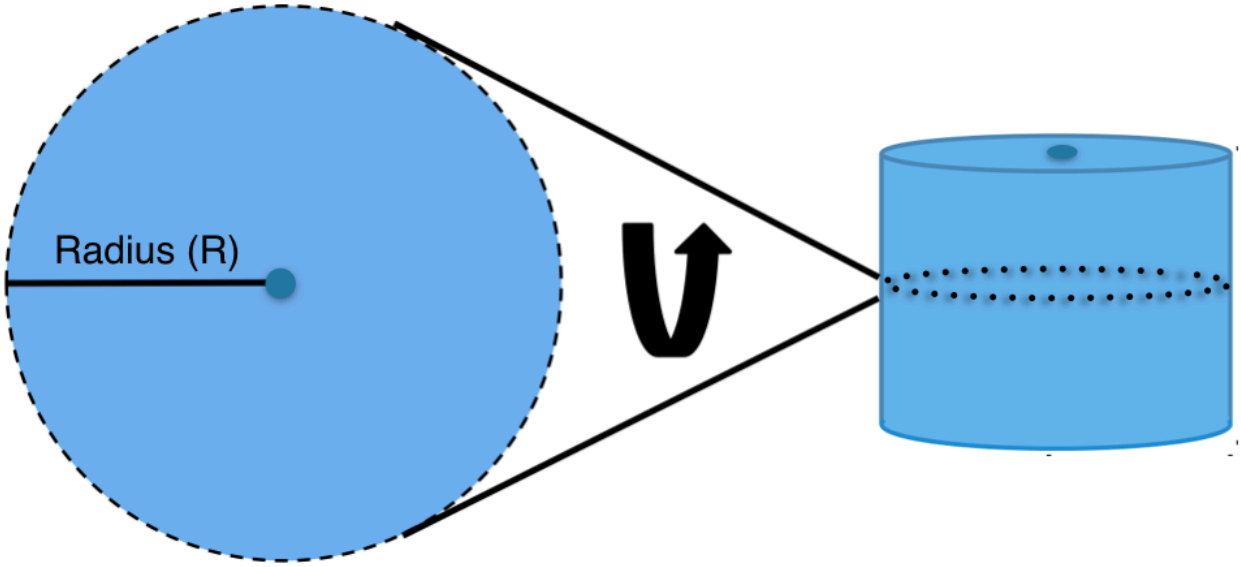

(b)

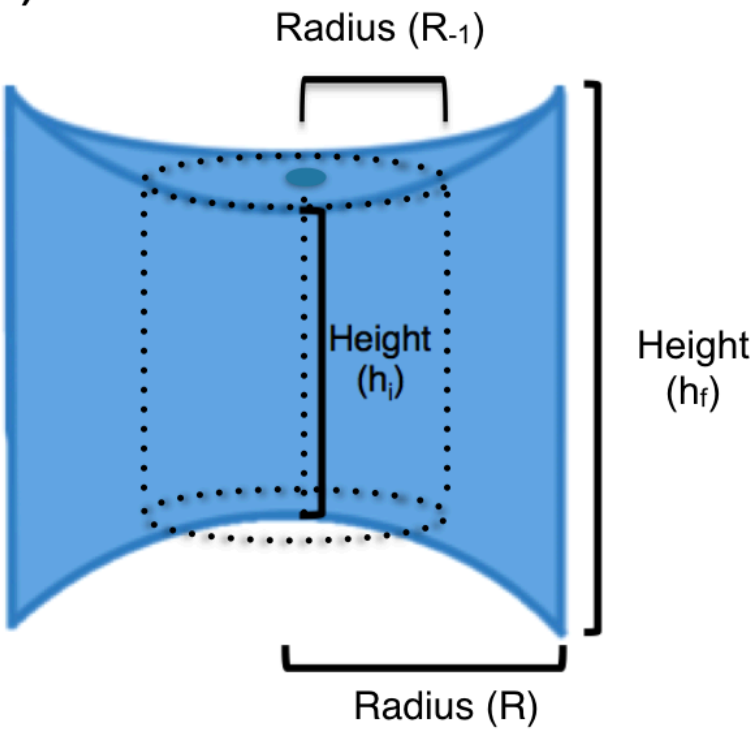

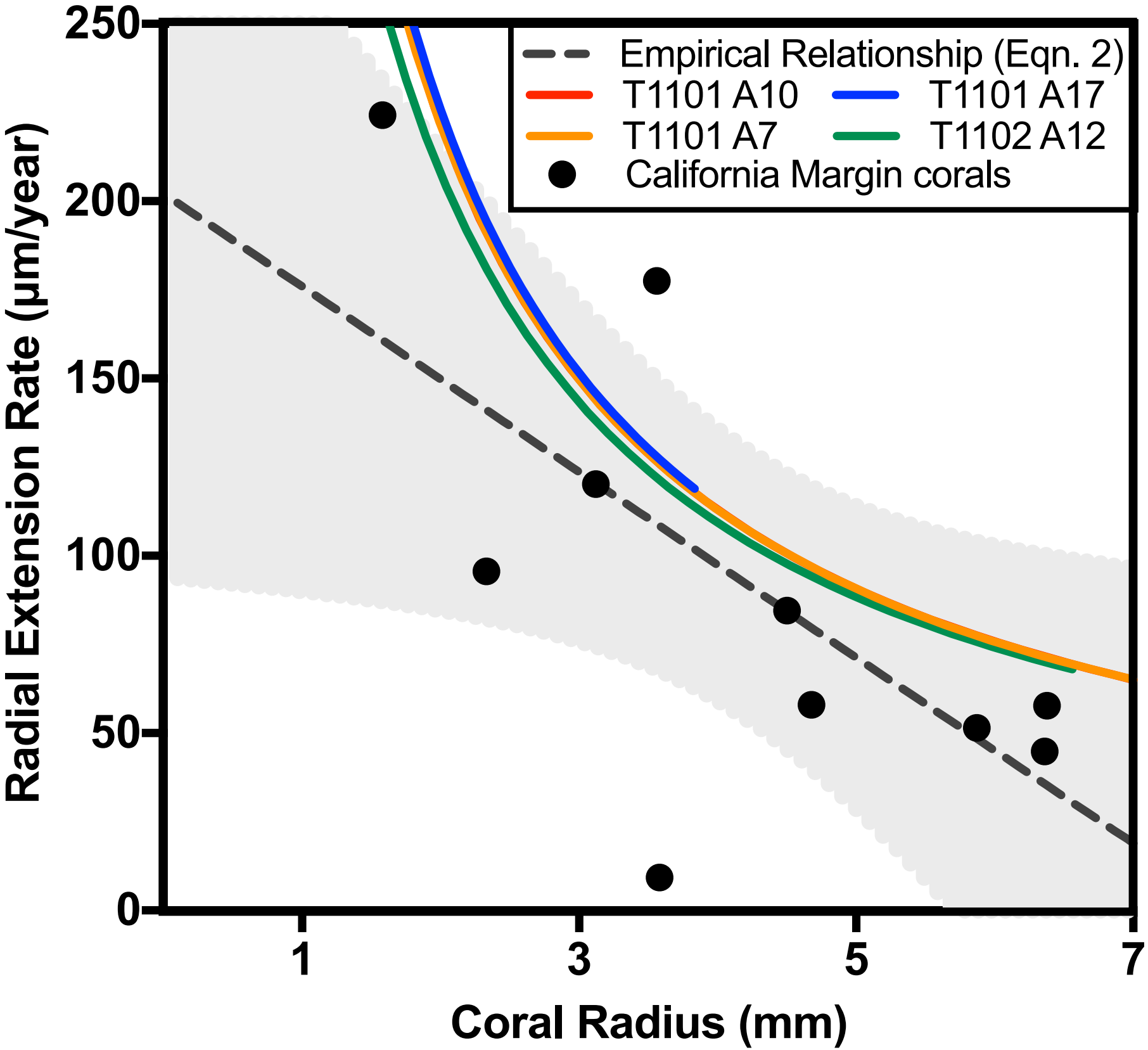
Empirical Relationship (Eqn. 2)
T1101 A10
T1101 A17
T1101 A7
T1102 A12
California Margin corals
Radial Extension Rate (µm/year)
250
200
150
100
50
0
1
3
5
7
Coral Radius (mm)

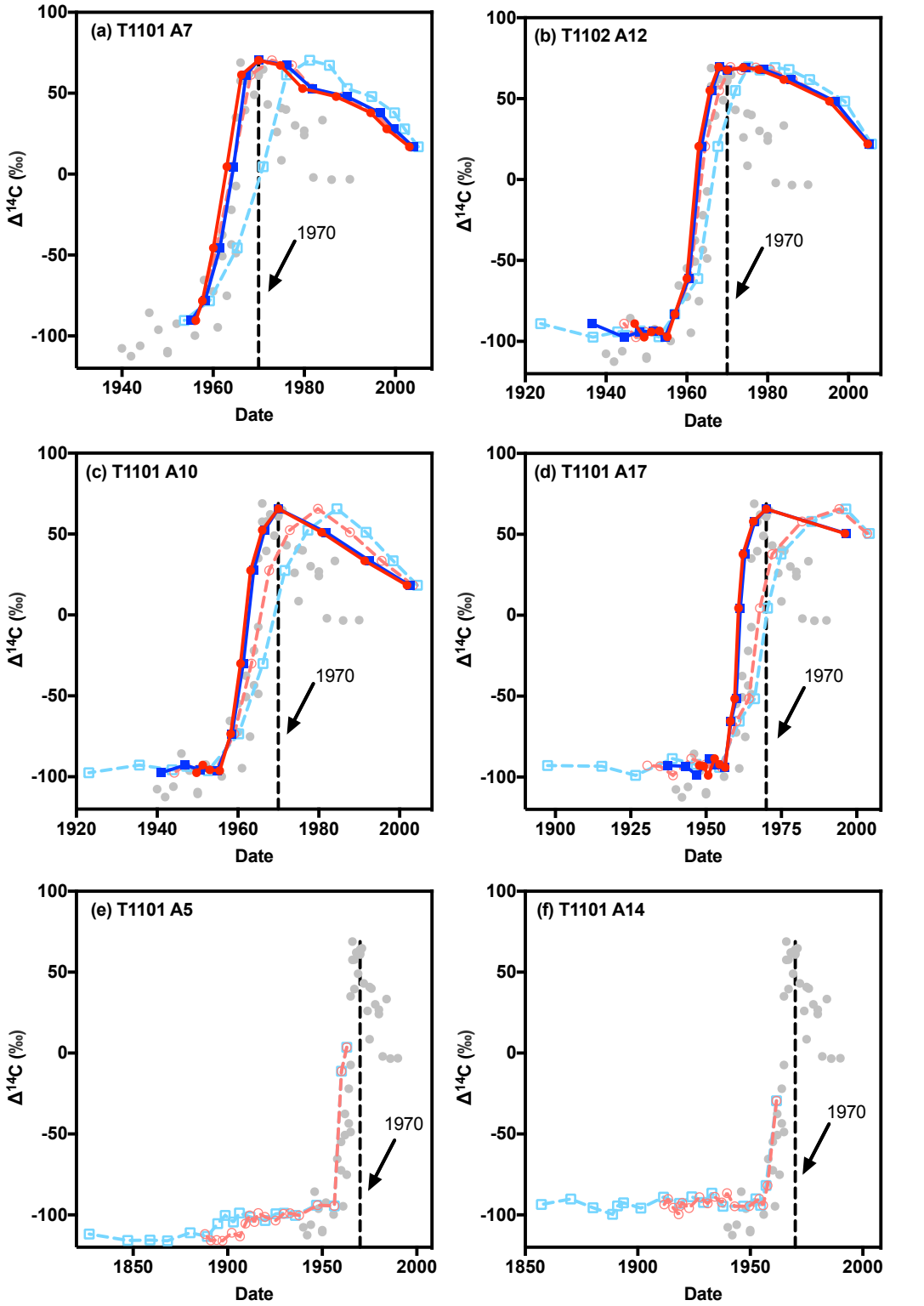
(a) T1101 A7
(b) T1102 A12
(c) T1101 A10
(d) T1101 A17
(e) T1101 A5
(f) T1101 A14
Δ14C (‰)
Date
1970
Area-based model (3 tie points)
Area-based model (2 tie points)
Kerr et al. (2004) yelloweye rockfish otolith
Linear interpolation (3 tie points)
Linear interpolation (2 tie points)

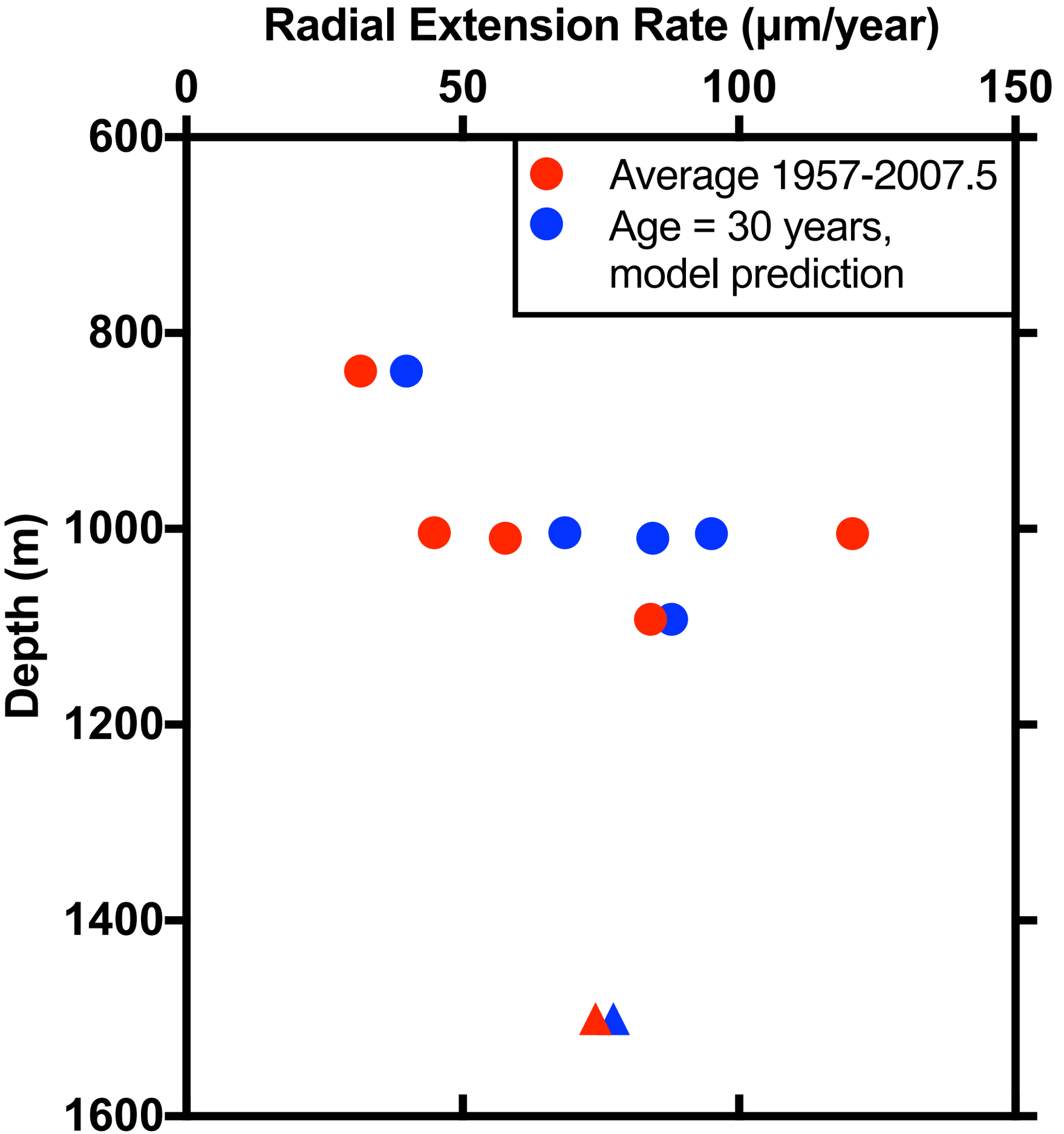
Radial Extension Rate (μm/year)
0
50
100
150
600
800
1000
1200
1400
1600
Depth (m)
Average 1957-2007.5
Age = 30 years,
model prediction

Table 1. Coral samples analyzed in this work, including samples from Sherwood et al. (2009) denoted by "**".

Coral ID	Species	Sample type	Live at collection?	Seamount	Depth (m)	Year Collected	Latitude	Longitude	Overall node radius (mm)	Node sampling resolution (mm/peel)
T1101 A7	*Isidella*	base	Yes	Pioneer, CM	1005	2007	37° 22.368' N	123° 24.199' W	7.67	0.6 ± 0.2
T1102 A12	*Keratoisis*	base	Yes	Davidson, CM	1500	2007	35° 43.874' N	123° 43.563' W	6.86	0.4 ± 0.2
T1101 A10	*Isidella*	base	Yes	Pioneer, CM	1092.2	2007	37° 22.288' N	123° 24.390' W	7.80	0.6 ± 0.1
T1101 A17	*Isidella*	branch	Yes	Pioneer, CM	839	2007	37° 22.458' N	123° 24.972' W	3.92	0.3 ± 0.2
T1101 A5	*Keratoisis*	base	Yes	Pioneer, CM	1004	2007	37° 22.358' N	123° 24.212' W	6.67	0.3 ± 0.2
T1101 A14	*Isidella*	base	No	Pioneer, CM	1009.7	2007	37° 22.232' N	123° 24.552' W	6.85	0.3 ± 0.2
I4**	*Isidella*	base	Yes	Tasmanian Seamount	1140	2007	44° 19.799' S	147° 7.7999' E	7.18	0.8 ± 0.6
L4**	*Lepidisis*	base	Yes	Tasmanian Seamount	1140	2007	44° 0.000' S	146° 11.999' E	3.41	0.4 ± 0.3
T.H17442**	*Lepidisis*	bae	Yes	Cascade Plateau	1000	1990	44° 11.399' S	150° 30.000' E	4.15	0.6 ± 0.3

Table 2. Radial extension rates estimated by interpolation between tie points and by applying our mathematically-based model. Samples with incomplete $\Delta^{14}C$ profiles are denoted with "*".

Coral ID	RADIAL EXTENSION RATE								
	Linear interpolation (µm/year)			Area-based model (dA/dt; mm^2/year)			Volume-based model (dV/dt; mm^3/year)		
				2 tie points	3 tie points		2 tie points	3 tie points	
	1957-1970	1970-2007.5	1957-2007.5	(1957-2007.5)	(1957-1970)	(1970-2007.5)	(1957-2007.5)	(1957-1970)	(1970-2007.5)
T1101 A7	224 ± 48	85 ± 5	121 ± 5	3.5 ± 0.1	4.3 ± 0.9	3.2 ± 0.2	32 ± 1	36 ± 8	31 ± 2
T1102 A12	120 ± 26	58 ± 3	74 ± 3	2.3 ± 0.09	2.9 ± 0.6	2.1 ± 0.1	21 ± 1	25 ± 6	20 ± 1
T1101 A10	178 ± 38	52 ± 3	84 ± 3	3.0 ± 0.1	5 ± 1	2.2 ± 0.1	28 ± 1	50 ± 10	22 ± 1
T1101 A17	96 ± 21	9.3 ± 0.5	32 ± 1	0.62 ± 0.02	1.8 ± 0.4	0.2 ± 0.01	5.2 ± 0.2	15 ± 3	1.9 ± 0.1
T1101 A5*	45 ± 13	-	-	1.8 ± 0.07	-	-	17.7 ± 0.7	-	-
T1101 A14*	58 ± 29	-	-	2.8 ± 0.1	-	-	27 ± 1	-	-
	(1957-1980)	(1980-2007)	(1957-2007)	(1957-1980)	(1980-2007)	(1957-2007)	(1957-1980)	(1980-2007)	(1957-2007)
I4	134 ± 5	101 ± 7	116 ± 5	2.5 ± 0.3	3.7 ± 0.3	3.1 ± 0.1	21 ± 3	34 ± 3	28 ± 1
L4	66 ± 7	27 ± 2	45 ± 2	0.80 ± 0.08	0.51 ± 0.04	0.64 ± 0.03	6.6 ± 0.9	4.3 ± 0.3	5.3 ± 0.2
T.H17442*	47 ± 4	-	-	1.1 ± 0.04	-	-	9.14 ± 0.4	-	-